https://doi.org/10.5194/egusphere-2026-1092
Preprint. Discussion started: 18 March 2026

Mid-Triassic rhyolitic lavas and ignimbrites as markers of Eoalpine high-pressure metamorphism and large-scale lateral extrusion of Adria derived units at the edge of the European Alps

Matija Vukovski[1], Damir Slovenec[1], Mirko Belak[1], Branimir Šegvić[2], Ivan Mišur[1], Duje Smirčić[3], Marija Horvat[1], Duje Kukoč[1], Tonći Grgasović[1], Goran Slivšek[4]

[1]Department of Geology, Croatian Geological Survey, Zagreb, 10000, Croatia
[2]Department of Geosciences, Texas Tech University, Lubbock, 79409, Texas, U.S.A
[3]Faculty of Mining, Geology and Petroleum Engineering, University of Zagreb, Zagreb, 10000, Croatia
[4] Institute for Anthropological Research, Zagreb, 10000, Croatia

Correspondence to: Matija Vukovski (mvukovski@hgi-cgs.hr)

Abstract

Middle Triassic felsic volcanic rocks exposed at Margečan and in the Kjumberk area, located along the Periadriatic Fault System and the Mid-Hungarian Shear Zone, have long been assigned to the Southern Alpine domain and interpreted mainly in terms of their magmatic affinity. This study demonstrates that ignimbritic rhyolites from the Margečan area record a previously unrecognized high-pressure, low-temperature metamorphic overprint reaching blueschist-facies conditions. Phengitic muscovite compositions indicate peak pressures of ~1.1–1.2 GPa at temperatures around 300°C, providing the first evidence that these felsic volcanic rocks were involved in Eoalpine subduction-related metamorphism and represent a part of the Austroalpine units. In contrast, felsic volcanic rocks from the nearby Kjumberk area, although compositionally and temporally similar, show no evidence of overprint and retain their Southern Alpine affinity, thus outlining a first order tectonic boundary between the two areas. U–Pb zircon ages constrain felsic volcanism to the late Anisian–early Ladinian (~244–242 Ma). Whole-rock geochemistry and Nd isotopic compositions indicate derivation from a subduction-modified mantle source with substantial crustal contribution, consistent with Triassic calc-alkaline magmatism along the Adriatic margin. These petrogenetic characteristics provide a framework for regional correlations but do not explain the contrasting metamorphic overprint. The recognition of Cretaceous Eoalpine blueschist-facies metamorphism in the Margečan ignimbrites therefore revises the tectonic interpretation of this sector of the Adriatic margin and implies large-scale eastward extrusion of the Austroalpine units into the Carpathian embayment, accommodated by high-offset right-lateral strike-slip faults.

1 Introduction

Continental collision and associated strong crustal thickening may lead to lateral extrusion processes, in which large blocks of the Earth's crust, ~~commonly high-pressure to high-grade crustal units metamorphosed~~, accreted and thickened in

https://doi.org/10.5194/egusphere-2026-1092
Preprint. Discussion started: 18 March 2026

subduction-collision settings, are displaced laterally away from the collision zone, typically along lithosphere-scale strike-slip faults. A prime example ~~are~~ the Eastern Alps, where the ALCAPA (Alps–Carpathians–Pannonia) unit (sensu Schmid et al., 2008) was extruded eastward during Alpine collision due to indentation of the Adriatic plate into Europe (Fig. 1a; Ratschbacher et al., 1989, 1991; Frisch et al., 2000; Wölfler et al., 2011). The study area in northern Croatia and eastern Slovenia ~~lies~~ along the southern boundary of this extruding wedge, defined by the right-lateral Periadriatic Fault System (PFS) in the Alps and its eastern continuation, the Mid-Hungarian Shear Zone (MHZ), which extends across the Pannonian Basin toward the Carpathians (Fig. 1a, b).

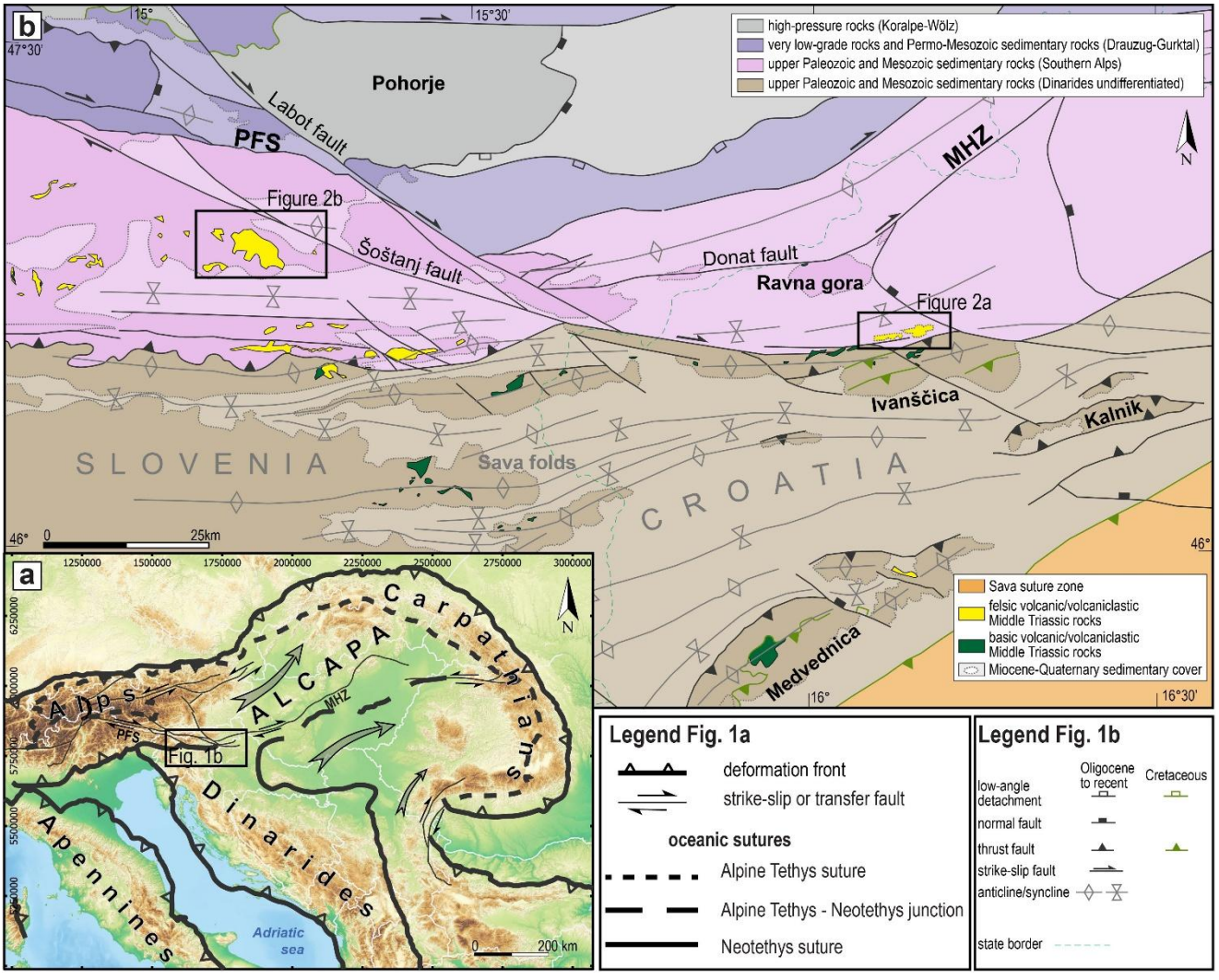

Figure 1 (a) Topographic map of the Alpine-Carpathian-Dinaridic orogen and Pannonian Basin region. Major tectonic boundaries after Schmid et al. (2020). **(b)** Tectonic map showing pre-Miocene tectonic units of the Dinarides and the Alps exposed from beneath the Neogene–Quaternary sedimentary cover (semi-transparent) after Schmid et al. (2020) and Fodor et al. (2021) modified according to Vukovski et al. (2024). Locations of Middle Triassic igneous and pyroclastic rocks, outlines of Miocene to Quaternary sediments, locations and age of folds and faults are compiled after Tomljenović & Csontos (2001), Fodor et al. (2021), Basic Geological Maps of former Yugoslavia on the 1:100,000 scale, sheets Klagenfurt (Buser and Cajhen, 1977), Kranj (Grad and Ferjančič, 1974), Ravne (Mioč et

https://doi.org/10.5194/egusphere-2026-1092
Preprint. Discussion started: 18 March 2026

al., 1981), Ljubljana (Premru, 1982), Slovenj Gradec (Mioč and Žnidarčič, 1976), Celje (Buser, 1977), Rogatec (Aničić and Juriša, 1984), Varaždin (Šimunić et al., 1982), Zagreb (Šikić et al., 1977) and Ivanić grad (Basch, 1981).

Despite the well-documented presence of ~~extrusion wedge high-offset boundary faults~~ in the study area (Fig. 1b; Schmid et al., 2008, 2020; Fodor et al., 2021), correlations between the rock units exposed in northern Croatia and potentially fault-offset correlative rocks along the boundary faults in Slovenia remain poorly constrained. Key reasons for this include uncertain magmatic affiliation and unresolved tectonic provenance of volcanic rocks exposed along major faults in this peripheral and significantly less studied segment of the Alpine and Dinaridic orogen, largely owing to the absence of constraints on their metamorphic evolution. In northern Croatia, at the transition between the PFS and the MHZ (Fig. 1b), a narrow and elongated body of felsic volcanic and pyroclastic rocks, originally documented during early geological mapping and described as Middle Triassic silicified tuffs (Fig. 2a; Šimunić et al., 1982), represents the last major, previously unstudied occurrence of Middle Triassic pyroclastic rocks. The tectonic position of the investigated rocks, combined with their previously unconstrained metamorphic history, has left their affiliation with either the non-metamorphic Southern Alpine domain or the metamorphic Austroalpine units unresolved.

This study aims to provide a detailed mineralogical and petrological account of Middle Triassic pyroclastic rocks (Šimunić et al., 1982) from the Margečan area in northern Croatia and potentially fault-offset correlative Middle Triassic felsic lavas (Buser, 1977) near Kjumberk Hill in eastern Slovenia. Through an integrated approach combining petrography, mineral chemistry, and in situ U–Pb zircon geochronology, the age, genetic relationships, and tectonic provenance of these lithologies were investigated to assess their links to regional tectonic units. Particular emphasis is placed on their tectono-metamorphic evolution, current structural context, and significance for post-rift orogenic processes and lateral extrusion–related crustal deformation in the Alpine–Carpathian–Dinaridic system, with high-pressure metamorphic overprint as the key criterion distinguishing Southern Alpine from Austroalpine units.

2 Geological Framework

Felsic pyroclastic rocks were investigated immediately north of Mt. Ivanščica within a prominent fault zone ~~striking~~ between the villages of Margečan and Prigorec in northern Croatia (Fig. 2a), whereas felsic volcanic rocks were studied in the Kjumberk Hill area of eastern Slovenia, north of the village Velika Pirešica (Fig. 2b).

The investigated localities belong to the eastern segment of the tectonostratigraphic unit of the Southern ~~Alps~~ (Fig. 1b; Schmid et al., 2008). This unit is characterized by lithologies derived from the northern to northeastern Adriatic passive continental margin and its ~~basement~~ which were subsequently deformed by Miocene southward-directed thrusting and nappe stacking (Schmid et al., 2004, 2008, 2020). At that time, the study area occupied the eastern margin of the Alpine orogen, transitioning into the Pannonian Basin, which was characterized by synchronous extensional tectonics (Tomljenović and Csontos, 2001; Balázs et al., 2016; Fodor et al., 2021). This specific tectonic position resulted in complex deformation, characterized by ~~the~~ strong right-lateral displacements along the PFS and MHZ, ~~and by~~ low- to high-angle normal faulting

https://doi.org/10.5194/egusphere-2026-1092
Preprint. Discussion started: 18 March 2026

(Ratschbacher et al., 1989; Tomljenović and Csontos, 2001; Fodor et al., 2021). Prior to these events, Mesozoic lithologies from the study area were affected by ~~the~~ Dinaridic Early Cretaceous (Vukovski et al., 2024) and Paleogene ~~southwest-ward~~ thrusting phases (Tomljenović et al., 2008; van Gelder et al., 2015; Žibret and Vrabec, 2016). By contrast, the northernmost parts of the Adriatic passive margin underwent ~~significantly~~ different tectonometamorphic evolution. These rocks were affected by tectonic processes related to the Cretaceous Eoalpine and ~~the following~~ Cenozoic ~~main~~ Alpine orogenic stages (Schmid et al., 2008, 2013; Handy et al., 2010, 2015). Today, these mostly high-pressure metamorphic Austroalpine units are juxtaposed against predominantly non- to low-grade metamorphic Southern Alpine units along the PFS and ~~MHZ~~ (Fig. 1b).

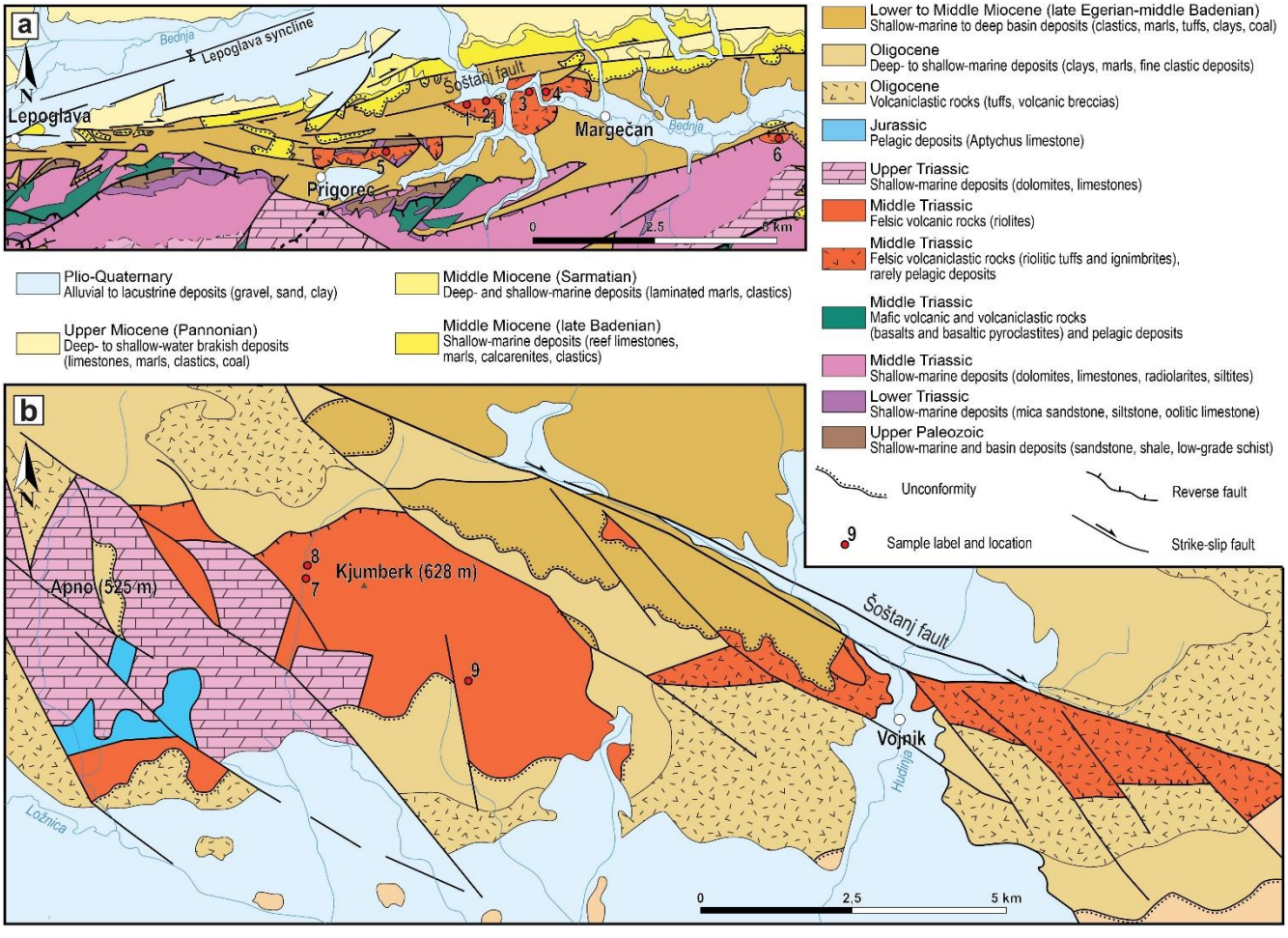

Figure 2 (a) Simplified geological sketch map of the northern Mt. Ivanščica and Margečan area in N Croatia (modified after Šimunić et al., 1982 and Vukovski et al., 2024). **(b)** Simplified geological sketch map of the wider Kjumberk Hill area in the eastern Slovenia (modified after Buser, 1977). Sample location: 1 = TSI-7, TSI-7A; 2 = MA-1, MA-2, MA-3, MA-4, MA-5, MA-6, MA-7, MA-8, MA-9, MA-10, MA-11; 3 = MA-12, MA-13, MA-14, MA-15, MA-16; 4 = MA II-1, MA II-2, MA II-3, MA II-4, MA II-5, MA II-6, MA II-7, MA II-8, MA II-9, MA II-10; 5 = GV-79; 6 = GK-1016; 7 = GA-2, 8 = GA-1; 9 = GA-3, GA-3A.

https://doi.org/10.5194/egusphere-2026-1092
Preprint. Discussion started: 18 March 2026

Large cumulative dextral displacement along PFS and MHZ, estimated from tens to several hundreds of kilometers (Tari, 1994; Fodor et al., 1998, 2001; Sachsenhofer et al., 2001), was in the study area accommodated by the Šoštanj, Lavant and Donat faults (Fig. 1). Their activity from the Miocene to recent times is well constrained (Frisch et al., 2000; Rainecker, 2000; Vrabec and Fodor, 2006; Weber et al., 2006; Fodor et al., 2008; Wölfler et al., 2010; Kurz et al., 2011; Grünthal and Wahlström, 2012; Stucchi et al., 2012; Atanackov et al., 2021; Bagagli et al., 2022; Prince et al., 2025). The investigated localities are situated within the southeasternmost segment of the PFS and its transition into the MHZ (Fig. 1). The Margečan locality lies within the Šoštanj fault zone, whereas Kjumberk Hill, located approximately 80 km to the west along strike, occupies the southern block of the same structure (Figs. 1 and 2).

In the Margečan area, the investigated pyroclastic rocks are predominantly bounded by steep fault contacts with Miocene sedimentary cover, and only locally are they unconformably overlain by lowermost Miocene siliciclastic deposits (Fig. 2a; Šimunić et al., 1982). In the vicinity of the Prigorec locality, felsic pyroclastic rocks are locally associated with Permian and Lower Triassic siliciclastic sandstone, as well as Middle Triassic shallow-marine carbonates and are outcropping from beneath the Lower Miocene clastic deposits (Fig. 2a; Šimunić et al., 1982). These rocks were tentatively assigned a Middle Triassic age (Šimunić et al., 1981, 1982), although earlier studies suggested a Lower Miocene age (Gorjanović-Kramberger, 1904) since relicts of both volcanic episodes are frequently found in the area. In the Kjumberk Hill area, the investigated felsic volcanic rocks are partly in fault contact with Upper Triassic shallow-marine carbonates and Upper Oligocene sediments, while along the southern margin of Kjumberk Hill, the felsic volcanic rocks are unconformably overlain by Upper Oligocene fine- to coarse-grained clastic deposits (Fig. 2b; Buser, 1977).

Middle Triassic volcanic and pyroclastic rocks are widespread in the study area (Figs. 2a-b) and are dominated by basic to intermediate lithologies with subordinate felsic varieties, usually intercalated with radiolarites, pelagic carbonates and siliciclastic sediments (Germovšek, 1953, 1959; Buser, 1977; Marci et al., 1982, 1984; Goričan et al., 2005; Slovenec et al., 2020, 2023; Slovenec and Šegvić, 2021; Kukoč et al., 2023; Smirčić et al., 2024). Felsic varieties become increasingly abundant toward the west, predominating over the basic and intermediate types (Fig. 1b). These volcano-sedimentary successions are generally interpreted as products of Middle Triassic rift-related magmatism along the eastern and northern Adriatic passive margin (Slovenec et al., 2020, 2023; Slovenec and Šegvić, 2021).

3 Materials and methods

3.1 Samples and analytical methods

Detailed field investigations were carried out in the study area, including systematic documentation of lithological features and deformation structures at all accessible outcrops, given that the terrain is covered by thick soil and dense vegetation. Thirty-five representative rock samples were selected for petrographic analyses (Appendix A). The rocks' petrographic characteristics were studied using an Optika B-1000 POL polarizing microscope equipped with a CP6-FL camera installed at University of Zagreb's Faculty of Mining, Geology and Petroleum Engineering.

https://doi.org/10.5194/egusphere-2026-1092
Preprint. Discussion started: 18 March 2026

Phase, chemistry of two representative samples was analyzed at the University of Geneva's Department of Earth Sciences using a JEOL JXA 8200 Superprobe equipped with five wavelength-dispersive spectrometers. Operating parameters included an accelerating voltage of 20 kV, a 15 nA beam current, and a defocused beam of ~10 µm. Counting times of 30 s on peak and 15 s on background on both sides of the peak were used for all elements, except for Na and K, which were measured 20 s and 10 s on peak and background, respectively, due to their high mobility under an electron beam. For this reason, Na and K were also measured first. Limits of detection (LOD) were calculated as the minimum concentration required to produce count rates three times higher than the square root of the background (3σ; 99 wt.% degree of confidence at the lowest detection limit). Concentrations below the LOD are reported as not detected. Raw data were corrected for matrix effects using the φρZ method by Armstrong (1991). Natural minerals, oxides (corundum, spinel, hematite, and rutile), and silicates (albite, orthoclase, anorthite, and wollastonite) were used for calibration. Mineral formulas were calculated using a software package MINPET, written by Linda R. Richard (Gatineau, Québec, Canada).

X-ray powder diffraction (XRD) was performed on the global particle fraction on a set of eight samples. Sample preparation included initial material powdering in an agate mortar prior to whole rock measurements. The measurements were undertaken at the Geosciences Clay Laboratory of Texas Tech University using a Bruker D8 Advance diffractometer. This instrument features a horizontal goniometer axis and synchronized rotation of both the X-ray source and detector arms. Measurements consisted of a step scan in the Bragg-Brentano geometry with CuK□□radiation (40 kV and 40 mA). Sample mounts were scanned for 1.8 s per 0.02°, from 3° to 70 °2θ. XRD traces interpretation was accomplished using Bruker EVA software and comparison against the PDF4 database issued by the International Centre for Diffraction Data.

Bulk-rock powders for chemical analyses of eleven samples were analyzed by X-ray fluorescence (XRF) for major elements, and inductively coupled plasma mass spectrometry (ICP-MS) for trace elements at Texas Tech University's Department of Geosciences and Actlab Laboratories. International mafic rocks were used as standards. Major element and trace element concentrations were measured with accuracy and precision better than ±1% and ±5%, respectively. It is 3σ at 10 times the detection limit.

Neodymium isotopic compositions of four bulk rock samples were measured at the Noble Gas Laboratory Pacific Centre for Isotopic and Geochemical Research, University of British Columbia using a Triton Plus mass spectrometer. Normalizing ratios of 146Nd/144Nd = 0.7219 were assumed. The 143Nd/144Nd ratio for the La Jolla standard was 0.5118451 ± 0.000010 (2σ). Total procedural blanks were ~150 pg. Python™ programing language (numpy package) was used to calculate the Monte Carlo propagation error through 10000 iterations for 143Nd/144Nd(t).

Two samples (Kjumberk Hill rhyolitic lava: GA-1 and Margečan rhyolitic ignimbrite: MA-11) were collected for zircon U-Pb geochronology. The zircons from the sample were extracted using the standard method of crushing, sieving, heavy liquid separation, magnetic separation and hand-picking at the Croatian Geological Survey. The ~20–30 zircon grains per sample were then mounted in epoxy, ground, and polished until their crystal centers were exposed. Zircon U-Pb isotopic measurements were performed by laser ablation–inductively coupled plasma mass spectrometry (LA-ICP-MS) at the Arizona LaserChron Center (ALC) in the Department of Geosciences at the University of Arizona following techniques

https://doi.org/10.5194/egusphere-2026-1092
Preprint. Discussion started: 18 March 2026

detailed in Gehrels et al. (2006, 2008) and Gehrels and Pecha (2014). Analyses used a Photon Machines Analyte G2 Excimer Laser attached to a Thermo Element2 HR single-collector ICP-MS. The U-Pb age for each analysis was then calculated using the ALC in-house software E2agecalc, and for concordant subsets, a weighted average age was calculated using Isoplot 4.15 (Ludwig 2011).

3.2 Phengite-based ~~metamorphic pressures~~

Metamorphic pressures were estimated using the phengitic mica barometer of Massonne and Schreyer (1987), which is based on the pressure-dependent incorporation of the Tschermak substitution in white mica. This substitution involves the coupled exchange of Si for Al in the tetrahedral site, accompanied by the substitution of Al for Mg or Fe in the octahedral site, expressed by the reaction: $Mg^{2+} + Si^{4+} \leftrightarrow 2Al^{3+}$. With increasing pressure, phengitic mica accommodates higher Si contents per formula unit, reflecting enhanced stability of the celadonitic component under high-pressure conditions. For a given temperature, the Si content of phengitic mica therefore provides a quantitative constraint on pressure. Calculations were performed using measured mica compositions normalized to 11 oxygens, applying the Massonne and Schreyer (1987) calibration at fixed temperatures to evaluate the pressure conditions recorded during mica crystallization.

In addition ~~to mica-based barometry derived from chemical compositions~~, metamorphic pressures were independently constrained using the b-axis parameter of K-white mica. The b-cell dimension of phengitic muscovite is known to increase systematically with pressure as a result of enhanced celadonitic substitution (Sassi and Scolari, 1974; Guidotti and Sassi, 1986; Kisch et al., 2006; Ferreiro Mählmann et al., 2012). The b-parameter is determined from the position of the $d(060,33\bar{1})$ reflection, following the relationship $b = 6 \times d(060)$, measured by X-ray diffraction and provides a semi-quantitative estimate of pressure across metamorphic regimes. This method relies on the documented linear relationship between the $d(060,33\bar{1})$ spacing and the celadonite content of white mica (Ernst 1963; Guidotti et al., 1989; Rieder et al., 1998). XRD traces were inspected in the 59–63 °2θ range, and b-cell dimensions were calculated using the WIN-METRIC v.3.0.7. refinement software (Bruker-AXS). The resulting b-parameter values provide an independent constraint on pressure conditions and serve to corroborate pressures inferred from phengitic muscovite chemistry based on Tschermak substitution.

4 Results

4.1 Petrography and mineral chemistry of rhyolitic lavas and rhyolitic ignimbrites

The rhyolitic lavas exhibit a porphyritic texture and a homogeneous structure. They are composed of plagioclase phenocrysts, which are commonly altered to fine-grained white mica and clay minerals, whereas the predominantly fresh K-feldspar phenocrysts contain only occasional altered inclusions (Figs. 3a–b). The groundmass is leucocratic and devitrified, made of fine-sized quartz and white mica crystals (Figs. 3a–e). Rhyolitic ignimbrites at the investigated locality reach thicknesses of up to 100 m and are represented by welded, laminated, flow foliated units and welded massive ignimbrites.

https://doi.org/10.5194/egusphere-2026-1092
Preprint. Discussion started: 18 March 2026

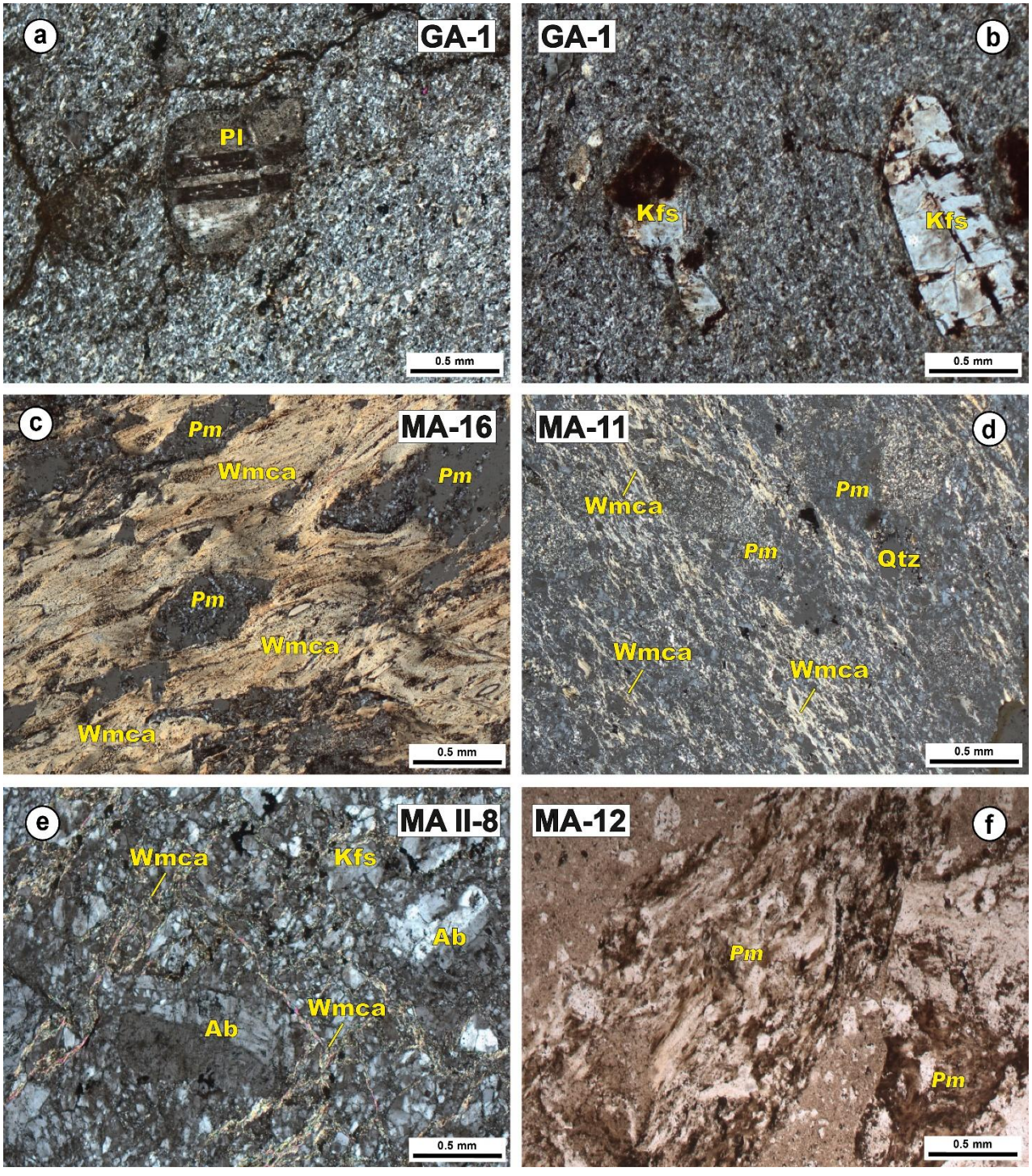

Figure 3 Micropetrographical characteristics of the Middle Triassic (a-b) rhyolitic lavas from the Kjumberk Hill (E Slovenia) and (c-f) rhyolitic ignimbrites from the Margečan area (N Croatia). Mineral abbreviations after Whitney and Evans (2010): Ab = albite, Kfs = alkali feldspar, Pl = plagioclase, Qtz = quartz, Wmca = white mica. *Pm* = pumice.

https://doi.org/10.5194/egusphere-2026-1092
Preprint. Discussion started: 18 March 2026

Foliated bands range from 1 to 10 cm in thickness and consist of alternating very thin layers of vitrophyric (Fig. 3c), crystaloclastic (Figs. 3d–e), and lapilli-bearing vitrophyric (Fig. 3f) rhyolitic pyroclastic flow material. Vitrophyric laminas of the rhyolitic pyroclastic flow are made of altered matrix-supported ash-sized pyroclastic detritus (< 2 mm in size) and a devitrified glassy groundmass. The vitrophyric lapilli bearing laminae contain altered matrix-supported to clast-supported pumice fragments larger than 2 mm, along with crystaloclasts embedded in a devitrified glassy groundmass (Fig. 3f). The crystaloclastic laminae of the rhyolitic pyroclastic flow are composed of quartz, albite (An0.0-4.5Ab95.1-99.9Or0.1-0.6; Figs. 3e, 4a; Appendix B) and K-feldspar (An0.0-1.0Ab1.8-4.2Or95.0-98.4; Figs. 3e, 4a; Appendix B) crystaloclasts, along with very rare pumice fragments, while the matrix is altered to white mica (phengite) exhibiting a conjugate tectonic cleavage texture (Fig. 3e). Welded rhyolitic lapilli ignimbrites exhibiting massive texture are made of clast-supported to matrix-supported altered lapilli-sized pumice fragments (> 2 mm), and less commonly of feldspar and quartz crystaloclasts, all set within a devitrified glassy groundmass (Fig. 3f). The alteration products in all varieties are fine-grained quartz and foliated phyllosilicates (Figs. 3c–e). The alteration is biphasic, having developed during (i) diagenetic processes and (ii) post-diagenetic tectonic overprinting, expressed as dynamo-thermal metamorphic alteration marked by a schistosity cleavage along which foliated white mica developed (Figs. 3d–e). The white mica may be classified as phengitic muscovite (Fig. 4) with a Si content of 3.4 a.p.f.u. (Appendix B). The undulose extinction of quartz crystaloclasts further indicates post-diagenetic dynamo-metamorphism to which the analyzed rocks were subjected to.

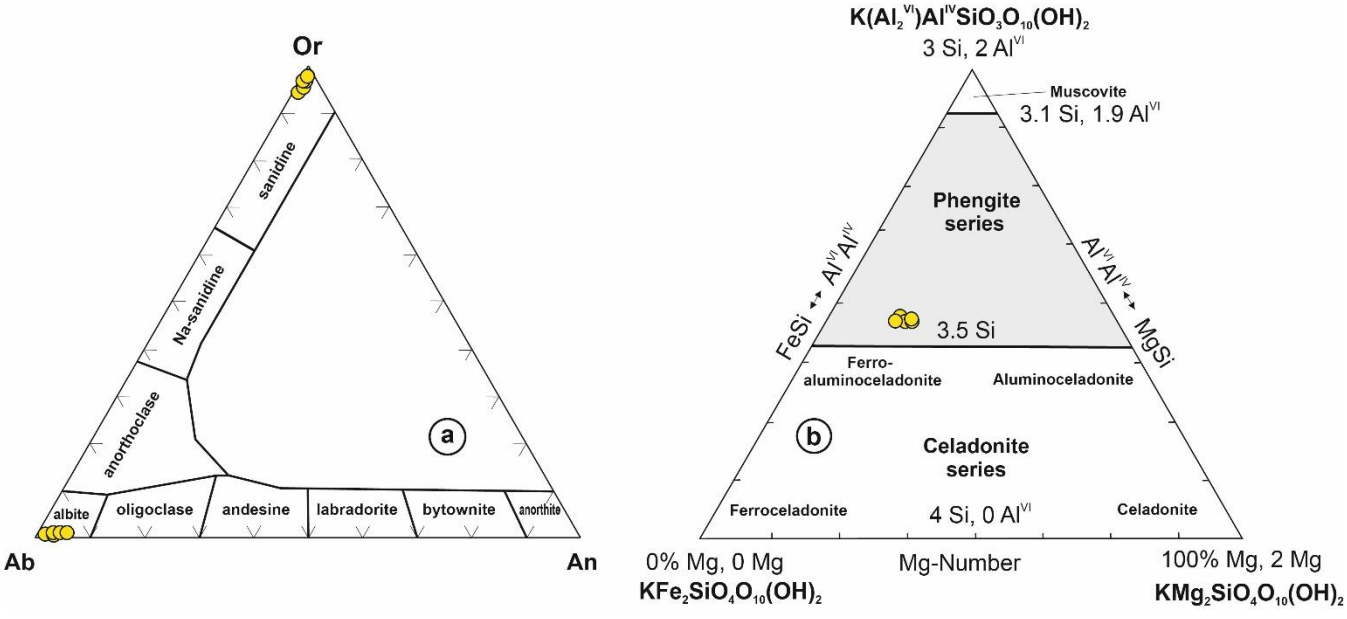

Figure 4 Classification diagrams for feldspar [Ab – An – Or plot; Deer et al. 1992; Dana et al. 1993] and mica [$K(Al_2^{VI})Al^{IV}SiO_3O_{10}(OH)_2$ – $KFe_2SiO_4O_{10}(OH)_2$ – $KMg_2SiO_4O_{10}(OH)_2$ plot; taken from Tappert et al., 2013] from the rhyolitic ignimbrites from the Margečan area (N Croatia).

X-ray diffraction mineralogy supports the petrographic observations described above, while also providing additional constraints on the extent of post-magmatic alteration. Quartz is the dominant crystalline phase in all investigated

https://doi.org/10.5194/egusphere-2026-1092
Preprint. Discussion started: 18 March 2026

rhyolitic ignimbrites and rhyolitic lavas, consistent with the quartz-rich groundmass and abundant quartz crystaloclasts observed in thin section (Appendix C). White mica occurs in all samples and locally reaches moderate relative abundances, reflecting pervasive alteration of the volcanic matrix and feldspar phases, as well as the development of cleavage-parallel phengitic muscovite documented petrographically and by EMPA. In contrast, K-feldspar is detected only in a limited number of samples and is absent from the majority of the investigated material. Its scarcity in the XRD patterns, despite petrographic evidence for apparently fresh K-feldspar phenocrysts, indicates that these phases are at least partially altered, most likely to fine-grained clay minerals such as kaolinite. Minor albite, kaolinite, and subordinate illite–smectite interstratifications occur sporadically, consistent with low-temperature alteration superimposed on the primary volcanic assemblage. Trace amounts of calcite and anatase were identified in a small number of samples and are interpreted as late-stage alteration products. XRD mineral assemblages corroborate the petrographic evidence for extensive devitrification of volcanic glass and confirm a biphasic alteration history involving early diagenetic processes followed by post-diagenetic tectonically controlled white mica formation.

4.2 Metamorphic pressure recorded in rhyolitic ignimbrites

Based on the white mica barometer of Massonne and Schreyer (1987), and assuming a metamorphic temperature of 300 °C (Kukoč et al., 2023; Vukovski et al., 2024), the estimated pressure ranged between 1.1 and 1.2 GPa. These values exceed the pressure conditions inferred from the b_0 lattice parameter of white mica (Appendix B), which yields moderate pressure estimates (b_0 = 9.04–9.08 Å). The b_0 lattice parameter data documented herein are, however, consistent with the values reported for a range of high-pressure, low-temperature (HP–LT) terrains (Iwasaki et al., 1978; Okrusch et al., 1978; Altherr et al., 1979; Frey et al., 1983; Schertl et al., 1991; Okay, 2002; Kisch et al., 2006). This behavior is characteristic of HP–LT terranes, in which white mica chemistry may preserve peak-pressure conditions, whereas the b_0 lattice parameter commonly reflects partial re-equilibration during exhumation, resulting in moderate b_0 values that nevertheless remain typical of HP–LT metamorphic belts (Kisch et al., 2006).

4.3 Bulk-rock chemistry of rhyolitic lavas and rhyolitic ignimbrites

Representative geochemical analyses of nine rock samples are provided in Appendix D. The chemical compositions of all analyzed lava and ignimbrite samples fall within similar ranges and will, therefore, be considered as a single group. Although relatively variable, silica concentrations are consistently high (SiO_2 = 69.41-82.07 wt.%). The rocks are characterized by moderately high Al_2O_3 contents (up to 12.51 wt.%) and low concentrations of TiO_2 (≤ 0.29 wt.%), Fe_2O_3 (≤ 4.41 wt.%), MgO (up to 1.27 wt.%), CaO (≤ 0.14 wt.%), and P_2O_5 (≤ 0.06 wt.%), while K_2O concentrations display a broad range (1.69–10.42 wt.%). The wide range of K contents partly reflects varying modal amounts of alkali feldspar phenocrysts, consistent with petrographic observations (Figs. 3b, 3e). In the classification diagram Nb/Y vs. Zr/TiO_2 x 0.0001 (Pearce, 1996), analyzed rocks are plotted in the field of subalkaline rhyolite (Nb/Y < 0.5; Fig. 5a), which corresponds to their major mineral assemblage. High-K content (Appendix D) coupled with high values of Ce/Yb and Ta/Yb

https://doi.org/10.5194/egusphere-2026-1092
Preprint. Discussion started: 18 March 2026

indicate calc-alkaline to shoshonitic affinity (Fig. 5b). Low concentrations of Ni (≤ 20 ppm) and Cr (≤ 49 ppm) are in line with the evolved, felsic character of the rocks (Wilson 1989). Elevated Zr contents, reaching up to 410 ppm, the concomitant decrease in Zr/Hf ratios with falling Zr abundance, and a negative correlation of both Zr and Hf with SiO2 (not shown) point to zircon fractionation and imply that the melts were zircon-saturated (Linnen and Keppler, 2002). Low- to moderate-level selective mobilization of certain large ion lithophile elements (LILE), such as Cs, Rb, and Ba, likely associated with secondary low-temperature alteration, has been identified (Fig. 6a1). These elements are thus excluded from further petrogenetic interpretation. In contrast, high field strength elements (HFSE), including Th, Nb, Ta, Ti, Hf, Y, as well as the rare earth elements (REE), appear unaffected by post-magmatic overprint and are considered to retain their original magmatic signatures (Appendix G and Fig. 6a1).

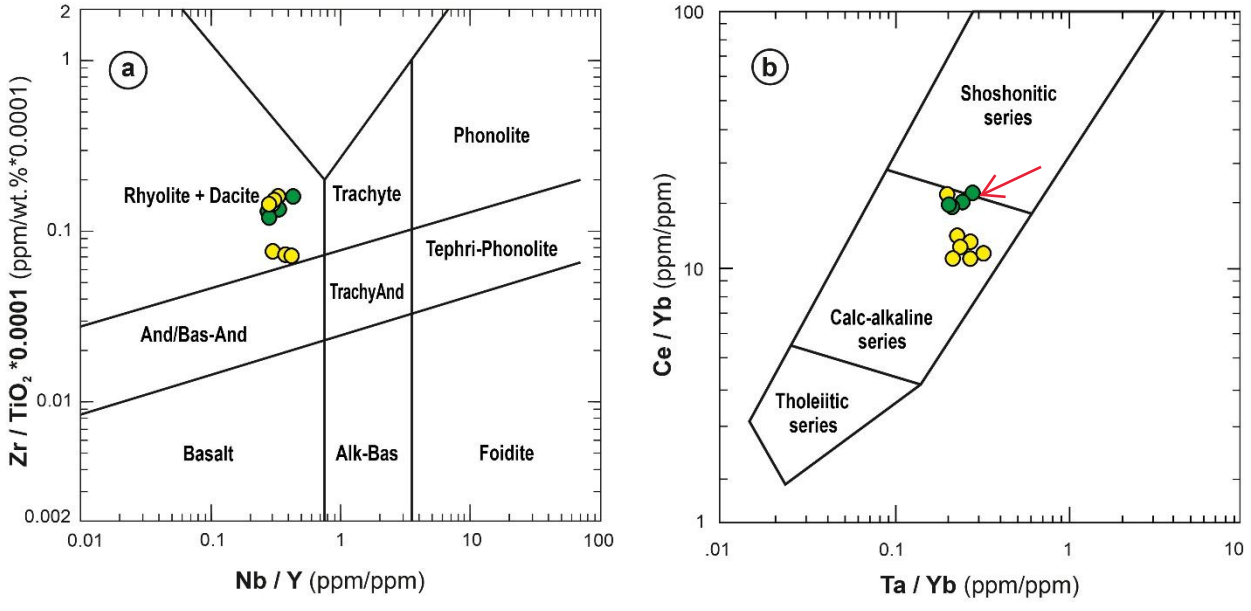

Figure 5 (a) Nb/Y – Zr/TiO_2*10^{-4} classification diagram (Pearce, 1996) and **(b)** Ce/Yb – Ta/Yb discrimination diagram after Pearce (1982) for the rhyolitic lavas (green dot) and rhyolitic ignimbrites (yellow dot) from the Margečan area (N Croatia) and Kjumberk Hill (E Slovenia).

In multielement spider patterns normalized to primitive mantle (PM) analyzed samples show enrichment in LILE (Cs, Rb, K) and Th (up to 1730 times relative to PM), strong negative anomaly of HFSE (Nb–Ta, P, Ti) and Sr [(Sr/Nd)PMN = 0.01–0.07] as well as variable positive Pb [(Pb/Ce)PMN = 1.64–11.92] and negative Ba [(Ba/Rb)PMN = 0.06–0.33] spikes (Fig. 6a1).

Chondrite-normalized REE patterns display fractionation and enrichment of light rare earth elements (LREE) over middle rare earth elements (MREE), with [(La/Sm)CN = 2.47–3.53] and total LREE concentrations ranging from 13 to 113 times chondritic values. This feature is more pronounced in the rhyolitic lava samples (Fig. 6b1). However, all samples exhibit an approximately flat pattern in the heavy rare earth elements (HREE), with [(Tb/Lu)CN = 0.86–1.53] and HREE concentrations ranging from 9 to 33 times chondritic values.

https://doi.org/10.5194/egusphere-2026-1092
Preprint. Discussion started: 18 March 2026

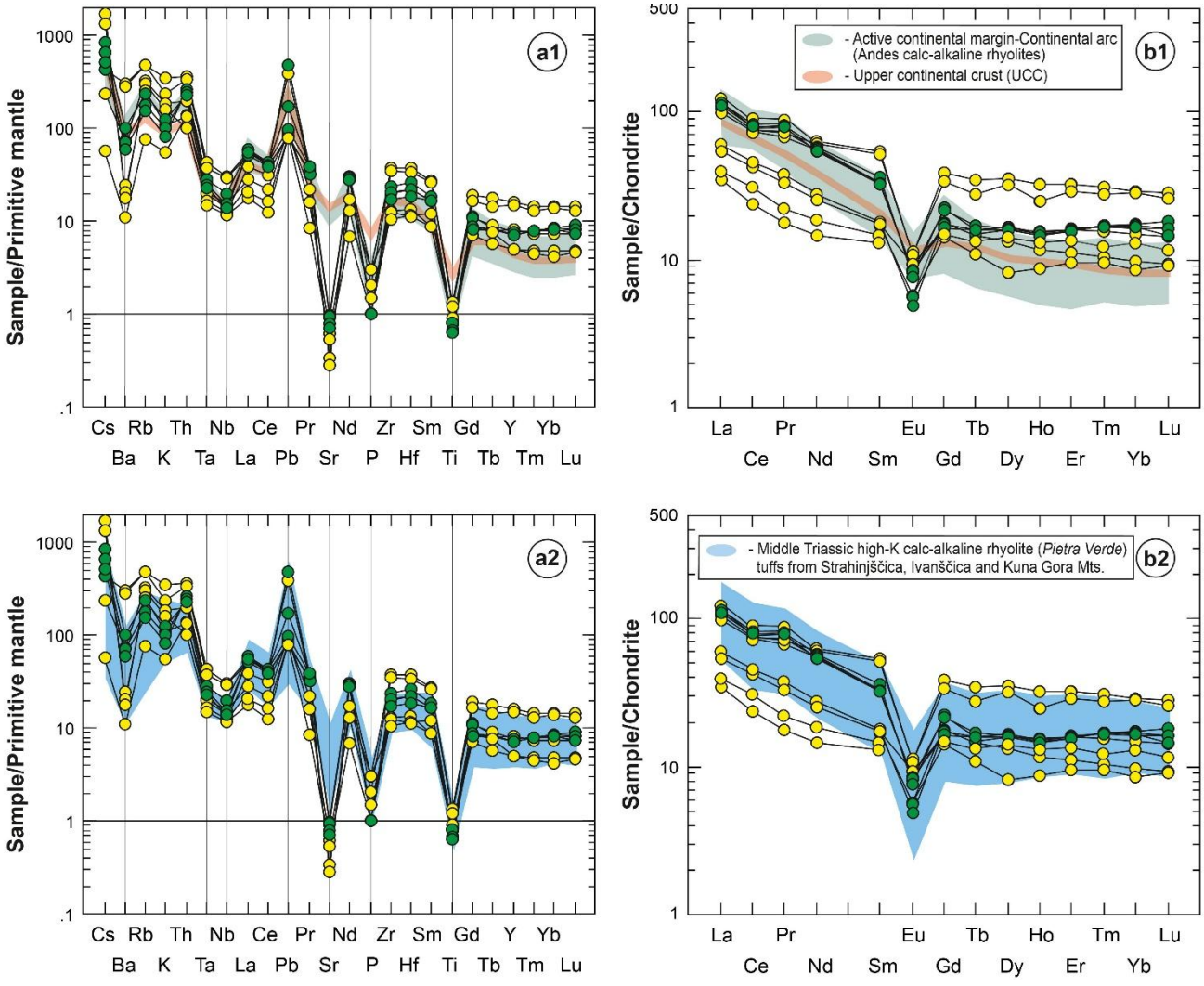

Figure 6 (a1, a2) Primitive mantle-normalised multielement and **(b1, b2)** REE patterns for the rhyolitic lavas (green dot) and rhyolitic ignimbrites (yellow dot) from the Margečan area (N Croatia) and Kjumberk Hill (E Slovenia). Normalisation values are from Sun and McDonough (1989) and Taylor and McLennan (1985). Pattern for upper continental crust (UCC; Rudnick and Gao, 2014), Andes calc-alkaline rhyolites (Riley et al., 2001; Garrison et al., 2011) and Middle Triassic high-K calc-alkaline rhyolitic tuffs from Strahinjščica, Ivanščica and Kuna Gora Mts. (Slovenec et al., 2023) are plotted for correlation constraints.

Measured 143Nd/144Nd ratios of four representative samples vary in a narrow range from 0.512250 to 0.512342 (Appendix E). The initial εNd are calculated for 242 and 243 Ma, the crystallization age of the analyzed rhyolitic lava and ignimbrite samples based on the U-Pb zircon dating (see below). The initial εNd varies between –4.42 to –5.13. Very low initial 143Nd/144Nd and εNd(t) values are close to the subducted continental material field and indicate a very high degree of crustal contamination (Fig. 7a). The influence of sedimentary and/or crustal components is further supported by the well-defined trend in the Th/La vs. Sm/La ratio (Fig. 7b).

https://doi.org/10.5194/egusphere-2026-1092
Preprint. Discussion started: 18 March 2026

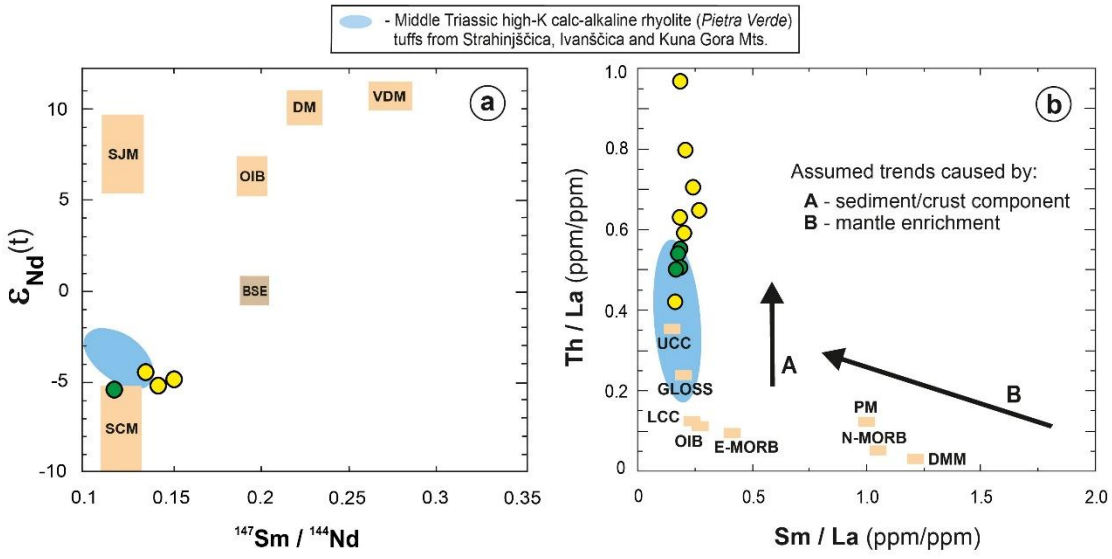

Figure 7 (a) $^{147}Sm/^{144}Nd$ – $\varepsilon_{Nd(t)}$ isotope ratios diagram for the rhyolitic lavas (green dot) and rhyolitic ignimbrites (yellow dot) from the Margečan area (N Croatia) and Kjumberk Hill (E Slovenia) [Hypothetical mantle sources: DM = depleted mantle (not refractory), VDM = very depleted mantle (refractory), SJM = subducted juvenile material (subducted oceanic crust; slab with little pelagic sediment), SCM = subducted continental material and BSE = bulk silicate earth. The observed compositions and hypothetical end members sources calculated for the Middle Triassic following Swinden et al. (1990)]. **(b)** Th/La – Sm/La diagram (after Plank, 2005) for the rhyolitic lavas (green dot) and rhyolitic ignimbrites (yellow dot) from the Margečan area (N Croatia) and Kjumberk Hill (E Slovenia). Abbreviations: [N-MORB = normal mid-ocean ridge basalts; E-MORB = enriched MORB; OIB = ocean island basalts; PM = primitive mantle (Sun and McDonough, 1989)]; [UCC = upper continental crust; LCC = lower continental crust (Rudnick and Gao, 2014)]; GLOSS = global subduction sediment (Plank and Langmior, 1998); DMM = depleted MORB mantle (Workman and Hart, 2005). Middle Triassic high-K calc-alkaline rhyolitic tuffs from Strahinjčica, Ivanščica and Kuna Gora Mts. (Slovenec et al., 2023) are plotted for correlation constraints.

4.4 U-Pb zircon dating of rhyolitic lavas and rhyolitic ignimbrites

The zircon grains from the Margečan rhyolitic ignimbrite (sample MA-11) range in size from 100 to 300 μm and are predominantly elongated, with sharp and straight grain boundaries. A total of 31 zircon grains were separated and analyzed for U-Pb dating from sample MA-11 (Appendix F). Of these, 26 analyses yielded concordant ages, while five were rejected as discordant, likely due to Pb loss or crystal alteration. The correction for initial Pb composition was not applied. The weighted mean age of the 26 selected zircon grains is 243.8 ± 0.43 Ma (MSWD = 12) (Fig. 8b).

A total of 22 analyses were performed on zircon grains from the rhyolitic lava sample GA-1 collected at Kjumberk Hill. The correction for initial Pb composition was not applied, and concordant ages were obtained from 21 out of 22 measurements. The results are presented in Appendix F and illustrated on the concordia diagram (Fig. 8a). The weighted mean age of these 21 selected zircons is 242.2 ± 1.80 Ma (MSWD = 0.23). The discordant age that was excluded may reflect Pb loss or crystal alteration. Additionally, three ages classified as concordant exhibit minor deviations from the concordia line but are still considered valid.

https://doi.org/10.5194/egusphere-2026-1092
Preprint. Discussion started: 18 March 2026

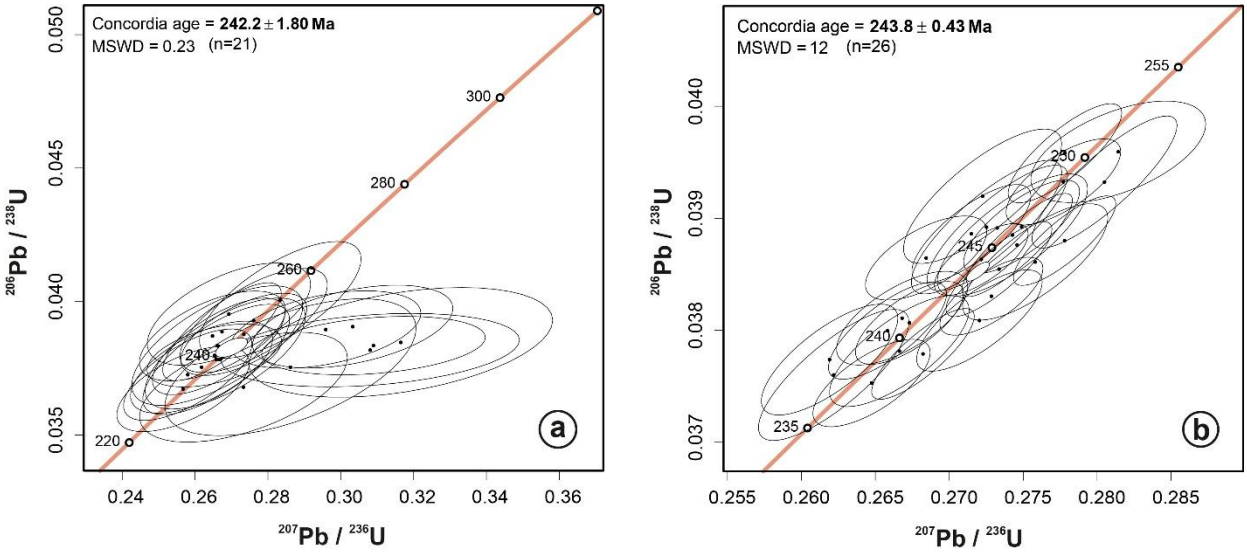

Figure 8 Concordia diagram and zircon U-Pb ages for the **(a)** Kjumberk Hill rhyolitic lava (sample GA-1) and **(b)** Margečan rhyolitic ignimbrite (sample MA-11). Discordant ages are not taken in to account.

5 Discussion

Mid-Triassic felsic pyroclastic rocks in the studied area are predominantly represented by Pietra Verde tuffs (Slovenec et al., 2023), whereas occurrences of rhyolitic lavas and welded rhyolitic ignimbrites are exceptionally rare. Unlike the effusive rhyolitic lavas, dominantly present in eastern Slovenia, the studied ignimbrites from the wider Margečan area in northern Croatia represent deposits formed by the emplacement of hot ash and vesiculated juvenile (pumiceous) clasts from pyroclastic density currents or pyroclastic flows (Cas and Wright, 1987; Branney and Kokelaar, 2002). Such flows consist of mixtures of gas and volcanic particles that move across the ground under the influence of gravity, typically generated by explosive volcanic eruptions (Burgisser and Bergantz, 2002). Rhyolitic eruptions are characteristic of continental settings and are commonly associated with partial melting of the continental crust, accompanied by magma differentiation, fractional crystallization, and crustal assimilation (Wilson, 1989; Halder et al., 2021).

Zircon U–Pb ages indicate that both, the Margečan rhyolitic ignimbrite (sample MA-11: 243.8 ± 0.43 Ma) and the Kjumberk Hill rhyolitic lava (sample GA-1: 242.2 ± 1.80 Ma) originated from a Middle Triassic magmatic event, spanning the late Anisian to early Ladinian. The overlapping analytical uncertainties suggest a potential genetic link between the two samples, implying derivation from the same magmatic system or tectonic setting. The relatively high MSWD value of 12 for sample MA-11 indicates that the age distribution displays greater scatter than expected for a single zircon population. This dispersion may reflect minor Pb loss, possibly related to the analysis of metamict domains, the presence of inherited zircon grains or cores, or unresolved analytical uncertainties. Nevertheless, the weighted mean age for sample MA-11 provides a reliable estimate of the primary magmatic crystallization age. In contrast, the low MSWD of 0.23 for sample GA-1 indicates

https://doi.org/10.5194/egusphere-2026-1092
Preprint. Discussion started: 18 March 2026

a coherent zircon population with minimal age dispersion, supporting the interpretation that these zircons crystallized during a single magmatic event with negligible post-crystallization disturbance. The slight discordance observed in three grains from GA-1, though within acceptable limits, may reflect minor Pb mobility. Nonetheless, the overall dataset is robust, and the close agreement between the two age populations suggests a broadly coeval magmatic episode. The marginally older age of the rhyolitic ignimbrite (243.8 ± 0.43 Ma) relative to the rhyolitic lava (242.2 ± 1.80 Ma) may imply that volcanism commenced with an explosive phase, followed by the effusion of rhyolitic lavas (Wadsworth et al., 2020).

5.1 Petrogenesis of rhyolitic lavas and rhyolitic ignimbrites

The very high SiO2 contents (> 79 wt.%) and elevated K2O concentrations (> 4 wt.%), coupled with low Na2O and CaO abundances and slightly higher loss on ignition (LOI = 2.02-3.83 wt.%), as well as the selective enrichment in Rb, Ba, and Cs (Appendix D; Fig. 6a1), suggest that some of the analyzed calc-alkaline to shoshonitic rhyolitic lavas and ignimbrites were affected by alteration processes of variable intensity, likely related to low-temperature hydration, hydrothermal activity, and/or low-grade metamorphism (Riley et al., 2001; Šegvić et al., 2023). The low K2O+Na2O (1.69-10.42) with a simultaneously extremely high ratio 100*K2O/(K2O+Na2O) (35.6-100.0), according to the criterion proposed by Hughes (1973), indicates weak to moderate K-metasomatism of the investigated rocks. In light of these characteristics, petrogenetic interpretations of the studied rocks are based on discrimination ratios of immobile trace elements, REE and Nd isotopic data.

The identical chemical and isotopic composition of the investigated Middle Triassic rhyolitic lavas and ignimbrites, along with the coeval acidic Pietra Verde tuffs identified in the broader study area (Slovenec et al., 2023), indicates a shared origin from the same magmatic source (Figs. 6a1–b1, 6a2–b2, 7a–b, 9a–b). The generation of these felsic volcanic rocks most probably involved partial melting followed by fractional crystallization of plagioclase and K-feldspar, as evidenced by the negative anomalies in Sr (Sr depletion, Xu et al., 2010) and Eu ((Eu/Eu* = 0.22-0.55); Figs. 6a1–b1; Slovenec et al., 2026), which represent key liquidus phases controlling melt composition (Storey, 1995). Feldspars in this crystallization system acted as stable residual phases, with crystallization taking place within the plagioclase stability field and in the absence of garnet (Wang et al., 2012; Fig. 9b). The magma from which these felsic rocks formed was subduction-related, as indicated by negative anomalies in Nb–Ta (e.g., Pearce et al., 1984; Hofmann, 1997) and probably Ti (Fig. 6a1), contaminated by lithospheric mantle melts, and sourced from a domain enriched in subduction-derived crustal components (Slovenec et al., 2026 in review). The crustal signature, more specifically the influence of subducted and recycled sediments, is reflected in (i) strongly negative initial εNd values (–4.42 to –5.13) accompanied by low $^{147}Sm/^{144}Nd$ ratios (≤ 0.134911; Fig. 7a), and (ii) a marked increase in Th/La at nearly constant Sm/La ratios (Fig. 7b). Partial melting of crustal rocks likely contributed to the genesis of these units, as suggested by chondrite-normalized REE patterns resembling those of the average upper continental crust (Fig. 6b1) and the presence of a positive Pb anomaly in the primitive mantle-normalized patterns (Fig. 6a1). The pronounced negative Eu anomaly may also carry a crustal signature (Rollinson, 1993; Rudnik and Gao, 2014; Fig. 6b1). This is characteristic of felsic magmas generated through partial melting of the upper continental crust (Wilson, 1989).

https://doi.org/10.5194/egusphere-2026-1092
Preprint. Discussion started: 18 March 2026

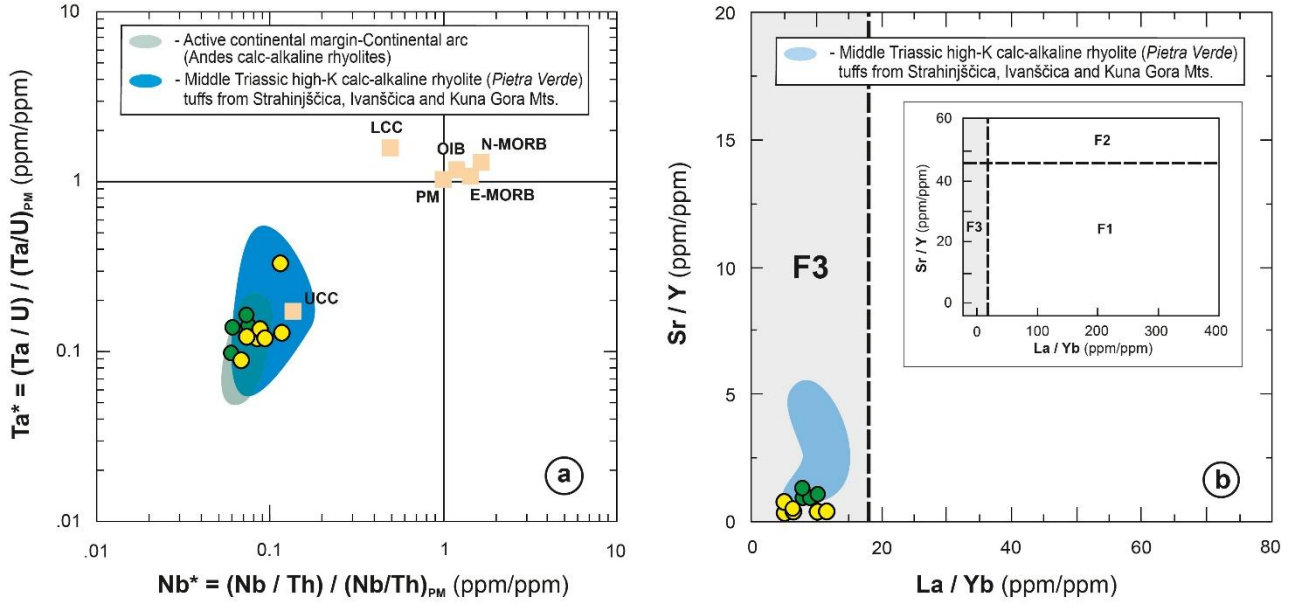

Figure 9 Discrimination diagrams for the rhyolitic lavas (green dot) and rhyolitic ignimbrites (yellow dot) from the Margečan area (N Croatia) and Kjumberk Hill (E Slovenia): **(a)** $(Nb/Th)/(Nb/Th)_{PM}$ – $(Ta/U)/(Ta/U)_{PM}$ plot (after Niu and Batiza, 1997; Niu et al., 1999). Abbreviations: [N-MORB = normal mid-ocean ridge basalts; E-MORB = normal mid-ocean ridge basalts; OIB = ocean island basalts; PM = primitive mantle (Sun and McDonough, 1989)]; [UCC = upper continental crust; LCC = lower continental crust (Rudnick and Gao, 2014)]. Data for Andes calc-alkaline rhyolites (Riley et al., 2001; Garrison et al., 2011) and Middle Triassic high-K calc-alkaline rhyolitic tuffs from Strahinjščica and Ivanščica Mts. (Slovenec et al., 2023) are plotted for correlation constrains. **(b)** La/Yb – Sr/Y plot (Halder et al., 2021 and references therein). Abbreviations: F1 = garnet stabillity field, little/no plagioclase, F2 = garnet and plagioclase stability field, F3 = plagioclase stability field, little/no garnet. Middle Triassic high-K calc-alkaline rhyolitic tuffs from Strahinjčica, Ivanščica and Kuna Gora Mts. (Slovenec et al., 2023) are plotted for correlation constrains.

It may be inferred that the origin of the Margečan rhyolitic ignimbrites and Kjumberk Hill rhyolitic lavas, genetically, temporally, and spatially associated with the Pietra Verde tuffs (Slovenec et al., 2023; Figs. 6, 7, 9), likely involved a combination of subduction-related mantle-derived melts and crustal magmas within a tectonic setting conducive to melting–assimilation–storage–homogenization (MASH) processes.

5.2 Tectonomagmatic and geodynamic implications

Felsic volcanic rocks may form in a variety of geotectonic settings. Gorton and Schandl (2000) and Pearce et al. (1984) proposed Ta/Yb vs. Th/Yb and Nb vs. Ta diagrams as effective tools for discriminating among them. Trace element ratios in the investigated rhyolitic rocks are analogous to those of felsic extrusive and pyroclastic rocks formed in an Andean-type continental margin volcanic arc (Riley et al., 2001; Garrison et al., 2011), and closely resemble those observed in the Pietra Verde tuffs from the broader study area (Figs. 10a–b). This interpretation is further supported by significant enrichment in LREE, selective depletion in HFSE, and pronounced negative anomalies in the Nb–Ta pair and probably Ti, all of which are characteristic of subduction-related settings (Pearce, 1982; Arculus and Powell, 1986; Hawkesworth et al., 1993; Figs. 6a1–b1). However, this does not necessarily reflect the actual tectonomagmatic setting of formation but is likely inherited from

https://doi.org/10.5194/egusphere-2026-1092
Preprint. Discussion started: 18 March 2026

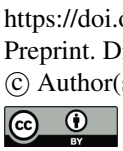

380 older (ancient) arc-derived lithologies associated with Paleotethyan subduction, which underwent partial melting (Slovenec and Šegvić, 2021; Slovenec et al., 2023). In addition, the consistent presence of a strong positive Pb anomaly and negative Eu anomaly in all samples (Figs. 6a1–b1) suggests that the magma might have formed in areas of mantle upwelling, such as continental rifts, settings where the Pb anomaly tends to be pronounced, in contrast to subduction zones, where it is typically weak or absent (Bachmann and Bergantz, 2008).

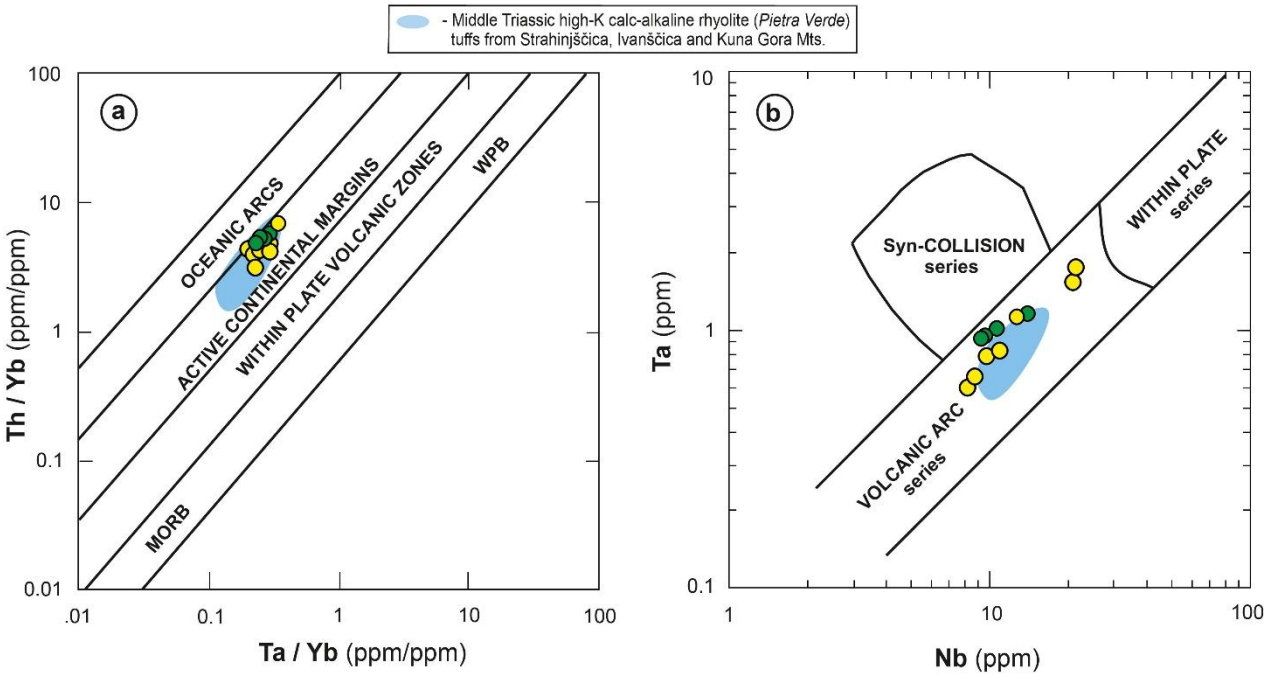

385

Figure 10 Discrimination diagrams for the rhyolitic lavas (green dot) and rhyolitic ignimbrites (yellow dot) from the Margečan area (N Croatia) and Kjumberk Hill (E Slovenia). **(a)** Ta/Yb – Th/Yb diagram (Gorton and Shandl, 2000). **(b)** Nb – Ta diagram (Pearce et al., 1984).

Considering the above interpretations, the origin of the studied rhyolitic rocks from the Margečan locality and 390 Kjumberk Hill can be understood within the geodynamic framework proposed by van Hinsbergen et al. (2020) and van Hinsbergen and Schouten (2021). These authors linked the opening of the Neotethys to the southwest-directed subduction of the Balkan Paleotethyan lithosphere beneath the northeastern margin of Greater Adria, followed by slab roll-back of the subducted Paleotethyan plate (Fig. 11a). This model favors passive continental rifting along the mid-Triassic northern margin of Greater Adria (Fig. 11b). Accordingly, the genesis of the investigated rocks involved: (i) partial melting of a 395 heterogeneous subcontinental lithospheric mantle that had been metasomatized during earlier Hercynian subduction events in the Late Paleozoic (Saccani et al., 2015), and (ii) to a lesser extent, processes related to crustal melting and fractional crystallization, as suggested by Slovenec et al. (2023). Effusions of rhyolitic lavas and explosive eruptions of pyroclastic (ignimbrite) flows occurred during the Middle Triassic along tectonically weakened zones of the rifted passive margin of Adria, forming basinal areas where such lithologies were alternating with the deposition of deep-marine siliciclastic and

https://doi.org/10.5194/egusphere-2026-1092
Preprint. Discussion started: 18 March 2026

carbonate sediments. One such short-lived basin, the Northwestern Croatian Triassic Rift Basin (Kukoč et al., 2023), located along the northeastern Adriatic passive margin (Fig. 11a), served as the site of this felsic magmatic activity during the late Anisian to early Ladinian.

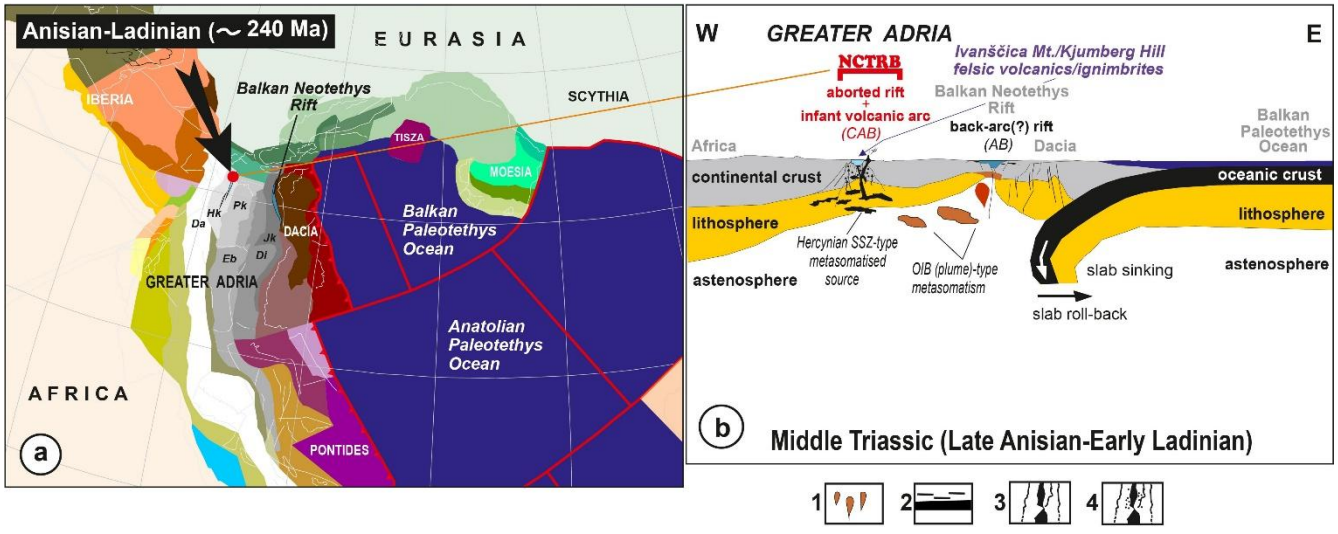

Figure 11 (a) The Anisian-Ladinian (~240 Ma) palaeogeographic reconstruction of the Mediterranean region simplified and slightly modified after van Hinsbergen et al. (2020) [Da = Dalmatian Nappe, Di = Drina-Ivanjica Nappe, Eb = East Bosnian-Durmitor Nappe, Jk = Jadar-Kopaonik Nappe, Hk = High-Karst Nappe, Pk = Pre-Karst Nappe] with location of investigated Margečan area (N Croatia) and Kjumberk Hill (E Slovenia) (marked with black arrow and red dot symbol). **(b)** Schematic geodynamic model (scale is approximate) for the central part of the Mediterranean region according to van Hinsbergen et al. (2020) palaeogeographic reconstruction shown in Fig. 11a. *CAB* = calc-alkaline and shoshonitic basalts/pyroclastites, *AB* = alkaline basalts, *OIB* = ocean island basalts; 1 = mantle diapires, 2 = oceanic crust topped by radiolarian cherts, 3 = partially melted previous subducted oceanic lithosphere, 4 = zone of partial melting and contamination by continental crust.

Given their closely matching ages and the clear geochemical similarity between the investigated rhyolitic lavas and the Pietra Verde tuffs from the broader study area in northern Croatia (Strahinjčica and Ivanščica Mts., Slovenec et al., 2023; Figs. 6-7, 9-10; Žumberak–Samoborska Gora Mts., Goričan et al., 2005; Fig. 1a), as well as with those from the External Dinarides (e.g., Donje Pazarište, Smirčić et al., 2018; vicinity of the town Gračac, Sokač et al., 1974; vicinity of the town Knin, Kuljak, 2004; Zelovo–Suvaja locality, Šćavničar et al., 1984), it can be inferred that the rhyolitic lavas and ignimbrites investigated in this study represent potential source, or one of the sources, of the Pietra Verde tuffs distributed along the northeastern passive margin of the Adria Plate (Fig. 11).

5.3 Metamorphic overprint and right-lateral extrusion tectonics

Felsic rock suites from both investigated localities, as well as the Middle Triassic Pietra Verde tuffs from the adjacent Ivanščica and Strahinjčica Mountains, share the same paleogeographic provenance, i.e., the northern to northeastern Adriatic passive margin. Consequently, their lithological characteristics, along with those of spatially and temporally associated units, are broadly similar and do not allow for clear discrimination into distinct tectonic units based solely on lithology. However, the three major tectonic domains that converge in the broader study area are characterized by diachronous orogenic histories,

https://doi.org/10.5194/egusphere-2026-1092
Preprint. Discussion started: 18 March 2026

and the pressure–temperature paths of the rocks composing these units differ significantly. Therefore, the distinct p-T evolution of each domain may serve as a key discriminant for distinguishing between rock units in the transitional zone between the Southern Alps, Dinarides and the Austroalpine units (Fig. 1b).

The maximum diagenetic temperature experienced by Middle Triassic rocks of the northern Dinarides and eastern Southern Alps in Slovenia reached up to 300°C, interpreted as the result of sedimentary burial, with peak thermal conditions attained during the Middle Eocene to Early Oligocene (Rainer et al., 2016). Assuming an average geothermal gradient of 25–30°C per kilometer, this corresponds to lithostatic pressures of approximately 0.3 GPa. Similar temperature conditions were recorded on Mt. Ivanščica, located 5 km to the south of the Margečan locality, where Mid-Triassic rocks also reached ~300 °C (Kukoč et al., 2023). However, in this case, the observed increase in thermal maturity was attributed to Early Cretaceous overthrusting and orogenic loading (Vukovski et al., 2024). Further westward, in the central Southern Alps, peak temperatures in Middle Triassic strata did not exceed 150 °C, corresponding to a maximum lithostatic pressure of ~0.15 GPa, related to Late Cretaceous to Paleogene sedimentary burial rather than tectonic loading (Grobe et al., 2015). In this context, the studied fresh, unmetamorphosed rhyolitic lavas from Kjumberk Hill are fully consistent with their current placement within the Southern Alps tectonic unit (Schmid et al., 2020). In contrast, the presence of phengitic muscovite in the rhyolitic ignimbrite from Margečan area (Appendices B and C) points to a significant overprint by HP–LT metamorphism, at conditions of 1.1–1.2 GPa and ~300°C, as suggested by phase chemistry and b_0 lattice parameter of white mica. These conditions sharply contradict the maximum p-T parameters recorded in the eastern Southern Alps and clearly exceed the pressure range required for the growth of phengitic muscovite under greenschist or burial metamorphic regimes. Instead, the observed assemblage corresponds to blueschist facies conditions, typical of subduction zones, and cannot be produced by any of the thermal regimes previously described for the Southern Alps. Although the timing of this metamorphic overprint remains uncertain, the only regional geodynamic event postdating the Mid-Triassic that could have generated blueschist facies metamorphism is the subduction associated with the closure of Neotethys. While the Dinarides dominantly preserve moderate- to high-pressure metamorphic assemblages related to high-temperature subduction-obduction processes (Šegvić et al., 2019, 2020), rare occurrences of HP–LT blueschist facies rocks have been reported from distal Adriatic margin units, such as the Mt. Medvednica (Belak and Tibljaš, 1998; Belak et al., 2026). Alternatively, the Austroalpine units of the Eastern Alps underwent intracontinental subduction and nappe stacking during the Cretaceous, culminating in high- to ultrahigh-pressure metamorphism around 95 Ma (Hoinkes, 1981; Faryad and Hoinkes, 2003; Thöni, 2006; Schmid et al., 2008; Janák et al., 2015). Considering the present-day regional tectonic position of the Margečan locality, it is the most plausible explanation that the rhyolitic ignimbrites are part of the northern Adriatic passive margin involved in the Eoalpine subduction system during the Cretaceous and consequently should be regarded as part of the Eoalpine high-pressure belt of the Austroalpine units (sensu Schmid et al., 2008) of the Eastern Alps (Fig. 12).

https://doi.org/10.5194/egusphere-2026-1092
Preprint. Discussion started: 18 March 2026

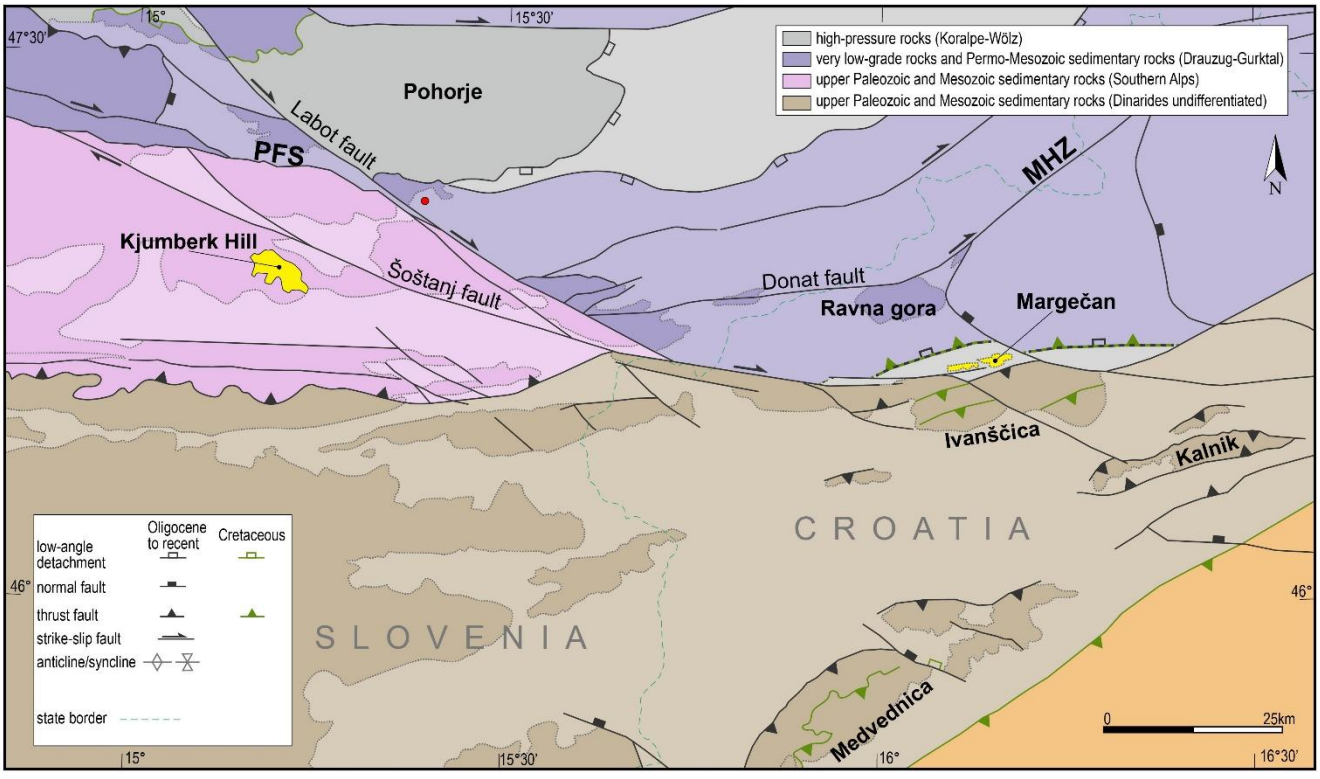

Figure 12 Tectonic map of pre-Miocene basement tectonic units exposed from beneath the Neogene–Quaternary sedimentary cover (semi-transparent) in the wider study area, after Schmid et al. (2020) and Fodor et al. (2021), modified according to Vukovski et al. (2024) and the results of this study. Lower to Middle Triassic clastic and carbonate rocks exposed at Mt. Ravna gora are according to their lithology and non- to very low-grade metamorphic overprint assigned to the Drauzug-Gurktal – structurally highest nappe system of the Austroalpine nappes. Margečan rhyolitic ignimbrites with blueschist facies metamorphic overprint are part of the Koralpe-Wölz nappe system characterized by Eoalpine high-pressure metamorphism. Structural boundary between these units may represent a Cretaceous thrust, or a Neogene low-angle extensional detachment, folded during Late Miocene to recent contraction. Inferred pre-extrusion (i.e., pre-Neogene) position of the Margečan ignimbrite is marked by red circle south of Mt. Pohorje.

During the Miocene, these segments of the Eoalpine high-pressure belt were laterally extruded eastward into the Carpathian embayment along major dextral strike-slip faults, most notably the Labot, Donat and Šoštanj faults, eventually reaching their current position in what is today northern Croatia. This is further supported by the recent discovery that the Oligocene to Lower Miocene sedimentary succession of the Hrvatsko Zagorje Basin (sensu Avanić, 2012; Avanić et al., 2021), exposed north of the Šoštanj Fault and representing sedimentary cover of Margečan ignimbrites, differs drastically from the succession exposed south of the same structure, and that it represents allochthonous units displaced to the present position from the west, where correlative units are exposed in Slovenia (Vukovski, 2024, Vukovski et al., 2024). Considering available kinematic constraints and estimated offsets along these strike-slip faults (Tari, 1994; Fodor et al.,, 1998, 2001; Sachsenhofer et al., 2001; Vukovski et al., 2024), a first-order reconstruction suggests that the pre-extrusion (i.e., pre-Neogene) position of the Margečan ignimbrite might have been located as much as 70 km to the W–NW along the fault (Fig. 12). This location is near the present-day position of the southern slopes of Pohorje Massif, which represents the closest

https://doi.org/10.5194/egusphere-2026-1092
Preprint. Discussion started: 18 March 2026

outcrops of the Eoalpine high-pressure belt rocks. This new finding indicates that the Austroalpine units were extruded much farther to the southeast than previously thought (Fig. 12), which has a direct impact on the amount of crustal stretching in the southernmost border of the extruding wedge, where during lateral extrusion, extension was predominantly accommodated by high-offset strike-slip faults.

6 Conclusions

The felsic volcanic and pyroclastic rocks from Margečan and Kjumberk Hill represent a significant addition to the understanding of Middle Triassic rift-related magmatism along the northern margin of Adria during the early stages of Neotethyan opening. Geochemical and isotopic data from the Late Anisian to Early Ladinian calc-alkaline to shoshonitic rhyolitic lavas and ignimbrites point to a magma source influenced by earlier (ancient) subduction processes, subsequently contaminated by lithospheric mantle melts and enriched by subduction-derived crustal components. The formation of these felsic volcanic rocks involved partial melting of a compositionally heterogeneous subcontinental lithospheric mantle, accompanied by subordinate melting of the continental crust and concurrent fractional crystallization of feldspar. The emplacement of rhyolitic lavas and ignimbrites occurred during passive continental rifting along the northern margin of Adria, contemporaneous with the development of a short-lived Northwestern Croatian Triassic Rift Basin. Based on their U-Pb zircon ages (~242–244 Ma) and geochemical affinity, these Late Anisian to Early Ladinian volcanic products likely represent one of the potential source regions for the widespread rhyolitic Pietra Verde tuffs observed across the Adriatic realm.

A key outcome of this study is the report of a high-pressure/low-temperature blueschist facies metamorphic overprint in the Margečan Middle Triassic ignimbrites. Although the rocks from both investigated localities share a common magmatic origin, their subsequent tectono-metamorphic histories diverge markedly. This divergence underlies the distinction of the Margečan and Kjumberk lithologies into two separate tectonic units. ~~Findings of~~ phengitic muscovite bearing assemblages indicate that Margečan rocks were subducted into the high-pressure metamorphic wedge, recording conditions of approximately 1.1 to 1.2 GPa and ~300 °C. In contrast, the Kjumberk rocks remained paleogeographically more distal to the subduction zone and thereby escaping high-pressure metamorphism. Consequently, these results indicate that the metamorphosed Margečan rocks are affiliated with the Eoalpine high-pressure belt of the Austroalpine units, whereas the Kjumberk Hill lavas show affinity with the Southern Alps.

The present location of metamorphosed Margečan ignimbrites is a consequence of Neogene eastward lateral extrusion of the ALCAPA block along the PFS and MHZ transfer zone. Within this zone, Šoštanj, Donat, and Lavant strike-slip faults accommodated major dextral displacements, enabling extrusion of Austroalpine high-pressure units far into the Pannonian Basin area in northern Croatia. This reconstruction extends the known southeastern limit of the Austroalpine units and has important implications for estimates of crustal stretching and fault displacements during lateral extrusion.

https://doi.org/10.5194/egusphere-2026-1092
Preprint. Discussion started: 18 March 2026

Appendix A: Overview of the studied rock samples from the Margečan area (N Croatia) and Kjumberk Hill (E Slovenia)

Table A1 Overview of the studied rock samples from the Margečan area (N Croatia) and Kjumberk Hill (E Slovenia).

Sample	Coordinates		Location (see Fig. 2)	Rock type	Analyses
	X	Y			
TSI-7	16.1132	46.1311	1	RIG	OM, XRD
TSI-7A	16.1132	46.1311	1	RIG	OM, CA, EMPA
MA-1	16.1132	46.1311	2	RIG	OM, XRD
MA-2	16.1132	46.1311	2	RIG	OM,
MA-3	16.1132	46.1311	2	RIG	OM,
MA-4	16.1132	46.1311	2	RIG	OM,
MA-5	16.1132	46.1311	2	RIG	OM,
MA-6	16.1132	46.1310	2	RIG	OM,
MA-7	16.1132	46.1310	2	RIG	OM,
MA-8	16.1131	46.1310	2	RIG	OM,
MA-9	16.1131	46.1310	2	RIG	OM
MA-9B	16.1131	46.1310	2	RIG	OM, XRD
MA-10	16.1131	46.1310	2	RIG	OM,
MA-11	16.1131	46.1309	2	RIG	OM, CA, Nd-isotopes, U-Pb
MA-12	16.1131	46.1309	3	RIG	OM,
MA-13	16.1131	46.1309	3	RIG	OM, XRD,
MA-14	16.1131	46.1309	3	RIG	OM, CA
MA-15	16.1131	46.1309	3	RIG	OM,
MA-16	16.1131	46.1309	3	RIG	OM, XRD
MA II-1	16.1152	46.1314	4	RIG	OM,
MA II-2	16.1152	46.1314	4	RIG	OM, XRD, CA
MA II-3	16.1152	46.1314	4	RIG	OM, XRD
MA II-4	16.1152	46.1314	4	RIG	OM,
MA II-5	16.1152	46.1314	4	RIG	OM,
MA II-6	16.1151	46.1314	4	RIG	OM,
MA II-7	16.1151	46.1315	4	RIG	OM,
MA II-8	16.1151	46.1315	4	RIG	OM, XRD, CA, EMPA
MA II-9	16.1150	46.1315	4	RIG	OM,
MA II-10	16.1150	46.1315	4	RIG	OM,
GV-79	16.1364	46.2051	5	RIG	OM, CA, Nd-isotopes
GK-1016	15.9983	46.1912	6	RIG	OM, CA, Nd-isotopes
GA-2	15.2028	46.3046	7	RI	OM, CA
GA-1	15.2029	46.3048	8	RI	OM, CA, U-Pb
GA-3	15.2032	46.3038	9	RI	OM, CA, Nd-isotopes
GA-3A	15.2032	466.3038	9	RI	OM, CA

Legend: RI = rhyolite, RIG = rhyolite ignimbrite; OM = optical microscopy, CA = chemical analyses, XRD = X-ray diffraction, EMPA = electronic microprobe analyses, U-Pb = zircon U-Pb isotopic dating.

Appendix B: Representative chemical compositions and calculated mineral formulae of alkali-feldspar, plagioclase and mica of rhyolitic ignimbrites from the Margečan area

Table B1 Representative chemical compositions and calculated mineral formulae of alkali-feldspar, plagioclase and mica of rhyolitic ignimbrites from the Margečan area.

Sample	TSI-7a	TSI-7a	TSI-7a	TSI-7a	TSI-7a	MA II-8	MA II-8	MA II-8	MA II-8	MA II-8	MA II-8	MA II-8	MA II-8
Anal. No.	3c	5r	10c	14c	16r	6c	7r	8c	9r	1c	2r	3	4
Species	*sa*	*sa*	*ab*	*ab*	*ab*	*sa*	*sa*	*sa*	*sa*	*phg*	*phg*	*phg*	*phg*
Oxides (wt.%)													

https://doi.org/10.5194/egusphere-2026-1092
Preprint. Discussion started: 18 March 2026

SiO_2	63.76	63.86	67.30	67.80	66.80	65.34	65.49	64.93	64.64	47.89	47.84	48.32	48.13
TiO_2	0.04	0.00	0.00	0.00	0.00	0.01	0.03	0.01	0.01	0.12	0.08	0.07	0.05
Al_2O_3	18.98	19.02	20.49	19.99	20.18	18.23	18.18	18.12	18.04	23.57	24.16	23.54	23.32
FeO	0.08	0.22	0.22	0.01	0.01	0.02	0.03	0.05	0.35	7.73	8.27	8.41	8.11
MnO	0.03	0.00	0.00	0.00	0.00	0.00	0.00	0.00	0.01	0.05	0.02	0.01	0.02
MgO	0.02	0.09	0.00	0.00	0.00	0.00	0.00	0.01	0.03	2.62	2.36	2.50	2.72
CaO	0.20	0.09	0.97	0.07	0.00	0.00	0.00	0.00	0.01	0.00	0.02	0.01	0.00
Na_2O	0.43	0.46	11.22	11.70	11.94	0.30	0.41	0.20	0.19	0.03	0.07	0.03	0.06
K_2O	15.79	15.56	0.08	0.10	0.02	15.28	15.15	15.40	15.29	10.69	10.41	10.17	10.59
Total	99.32	99.21	100.28	99.67	99.03	99.19	99.30	98.72	98.57	98.64	97.47	97.41	97.79
Calculated mineral formulae (a.p.f.u.)													
Si	2.966	2.968	2.942	2.973	2.955	3.022	3.024	3.020	3.015	3.401	3.380	3.413	3.399
Ti	0.001	0.000	0.000	0.000	0.000	0.000	0.001	0.000	0.000	0.006	0.004	0.004	0.003
Al_{tot}	1.040	1.041	1.055	1.032	1.050	0.993	0.989	0.993	0.991	1.973	2.012	1.959	1.941
Fe^{2+}	0.003	0.009	0.008	0.000	0.000	0.001	0.001	0.002	0.014	0.459	0.489	0.497	0.479
Mn	0.001	0.000	0.000	0.000	0.000	0.000	0.000	0.000	0.000	0.003	0.001	0.005	0.001
Mg	0.001	0.006	0.000	0.000	0.000	0.000	0.000	0.001	0.002	0.277	0.249	0.263	0.286
Ca	0.010	0.004	0.045	0.003	0.000	0.000	0.000	0.000	0.000	0.000	0.002	0.001	0.000
Na	0.039	0.041	0.951	0.995	1.023	0.027	0.037	0.018	0.017	0.004	0.010	0.010	0.082
K	0.937	0.923	0.004	0.006	0.001	0.902	0.892	0.914	0.910	0.969	0.938	0.916	0.954
Total	4.998	4.992	5.005	5.009	5.029	4.945	4.944	4.948	4.949	7.092	7.084	7.067	7.146
An	1.01	0.41	4.50	0.30	0.00	0.00	0.00	0.00	0.00	-	-	-	-
Ab	3.94	4.23	95.10	99.10	99.90	2.91	3.96	1.91	1.83	-	-	-	-
Or	95.02	98.41	0.40	0.60	0.10	97.10	96.02	98.12	98.20	-	-	-	-
$Fe^{2+}/(Fe^{2+}+Mg)$										0.62	0.66	0.65	0.62
P (GPa)*	-	-	-	-	-	-	-	-	-	1.2	1.1	1.2	1.2

Formulae calculated on the basis of 8 oxigens and total Fe as divalent for alkali-feldspar; 11 oxygens and Fe as divalent for mica. H_2O is calculated and corresponds to 2 (OH) per formula unit in mica; c = core, r = rim; *ab* = albite, *phk* = phengite; *sa* = sanidine. An = 100*Ca/(Ca+ N +K). *Massonne and Schreyer (1987).

Appendix C: Distribution and XRD relative abundances of primary and alteration phases in rhyolitic ignimbrites from the Margečan area

Table C1 Distribution and XRD relative abundances of primary and alteration phases in rhyolitic ignimbrites from the Margečan area. The last column provides b_0 values of phengitic muscovite.

Sample	Qtz	Kfs	Mica	Kln	I-S	Ant	Cal	b_o
TSI-7	++	+	*	+				9.0503
MA-1	++		+		*			9.0499
MA-9b	++		+		*			9.0514
MA-13	++		+		*			9.0586
MA-16	++		++		*	+	+	9.0473
MA II-2	++	+	+	+				9.0660
MA II-3	++		+	+			*	9.0588
MA II-8	++	++	+	+				9.0592

Abbreviations: Ab = albite; Cal = calcite; Ant = anatase; I-S = illite-smectite; Kfs = K-feldspar; Kln = kaolinite; Qtz = quartz; ++ = indicates major phases, + = indicates minor phases, * = indicates phases present, but not unequivocally confirmed by XRD. Mineral abbreviations after Whitney and Evans (2010).

https://doi.org/10.5194/egusphere-2026-1092
Preprint. Discussion started: 18 March 2026

Appendix D: Chemical compositions of ~~rhyolites and rhyolitic ignimbrites~~ from the Margečan area (N Croatia) and Kjumberk Hill (E Slovenia)

Table D1 Chemical compositions of rhyolites and rhyolitic ignimbrites from the Margečan area (N Croatia) and Kjumberk Hill (E Slovenia).

Sample	TSI-7a	MA-11	MA-14	MA II-2	MA II-8	GV-79	GK-1016	GA-1	GA-2	GA-3	GA-3A
Rock type	rig	rig	rig	rig	rig	rig	rig	ri	ri	ri	ri
Location	1	2	3	4	4	5	6	7	8	9	9
SiO_2	79.46	81.26	80.35	72.22	69.41	82.07	80.44	77.76	79.02	79.35	79.22
TiO_2	0.18	0.15	0.14	0.26	0.29	0.13	0.15	0.17	0.16	0.15	0.18
Al_2O_3	11.24	10.50	11.58	11.35	11.88	10.76	10.39	12.62	12.93	12.51	12.63
Fe_2O_{3total}	0.92	1.38	1.11	4.05	4.41	0.03	1.47	2.07	1.89	1.25	1.29
MnO	0.01	0.01	0.01	0.03	0.06	0.01	0.04	0.01	0.01	0.01	0.01
MgO	0.11	1.00	1.27	0.19	0.17	0.41	0.22	0.54	0.42	0.26	0.21
CaO	0.02	bdl	bdl	0.02	bdl	0.03	0.30	0.04	0.09	0.14	0.12
Na_2O	0.08	bdl	bdl	0.07	bdl	bdl	1.89	0.11	0.99	3.16	3.03
K_2O	5.59	3.28	2.88	7.25	10.42	1.69	3.25	2.51	3.01	1.75	1.56
P_2O_5	0.02	0.03	0.02	0.04	0.06	0.02	0.02	0.02	0.02	0.02	0.02
LOI	2.20	2.03	2.10	3.78	2.74	3.86	2.19	3.34	2.02	2.02	1.56
Total	99.83	99.63	99.46	99.26	99.46	99.05	100.36	99.19	100.56	100.62	99.83
Cs	1.9	10.8	13.7	4.1	3.5	0.5	2.9	4.1	5.2	6.7	6.2
Rb	177	124	132	306	309	48	136	157	112	152	144
Ba	250	246	325	1956	560	73	335	712	405	324	346
Th	17.2	11.3	8.7	28.5	30.9	11.7	21.7	22.5	21.04	19.6	19.8
Ta	0.80	0.84	0.61	1.56	1.77	0.67	1.10	1.17	1.03	0.96	0.95
Nb	9.8	11.0	8.2	20.7	21.4	8.8	13.0	13.9	10.6	9.6	9.8
Sr	14	13	11	19	21	17	15	17	16	17	16
Zr	231	146	139	395	416	218	256	270	223	195	199
Hf	6.8	4.1	3.4	10.5	11.5	3.6	7.4	8.1	6.8	5.8	5.6
Y	34.6	27.1	23.0	66.9	72.3	22.6	38.9	32.6	32.2	32.0	32.2
Sc	11	10	9	17	18	4	16	15	13	10	12
V	18	25	27	42	38	22	35	34	21	15	19
Cr	22	16	14	8	7	19	10	10	14	19	18
Ni	20	6	8	3	2	8	5	7	11	20	19
U	4.5	3.3	0.9	5.8	7.3	2.8	4.4	4.1	3.8	4.9	4.1
Pb	28.0	16.6	15.7	6.1	5.7	6.5	9	6.9	12.2	34.0	33.7
La	41.00	19.33	18.28	45.39	47.49	24.60	22.02	41.32	39.12	38.91	39.02
Ce	73.80	39.45	32.36	83.56	85.99	39.72	42.68	77.34	73.26	71.30	71.48
Pr	9.82	4.77	2.66	12.02	12.56	4.32	5.17	10.83	10.73	10.62	10.69
Nd	38.20	17.61	17.25	49.69	46.73	14.25	19.69	40.00	38.82	37.73	37.57
Sm	7.31	3.93	3.43	8.56	9.07	4.78	4.92	8.09	7.42	7.38	7.36
Eu	0.70	0.79	0.49	0.92	0.85	0.47	0.42	0.65	0.69	0.73	0.76
Gd	6.48	4.84	4.28	10.05	11.59	5.30	4.69	6.63	5.24	4.89	4.93
Tb	0.97	0.84	0.71	1.58	1.96	0.82	0.77	0.90	0.89	0.89	0.89
Dy	6.03	5.96	3.06	12.01	13.07	4.97	5.37	6.16	5.99	5.89	5.91
Ho	1.25	1.28	0.73	2.07	2.67	0.96	1.15	1.26	1.24	1.22	1.20
Er	3.91	3.85	2.32	6.98	7.86	2.69	3.37	3.87	3.81	3.77	3.79
Tm	0.58	0.54	0.33	0.97	1.07	0.36	0.43	0.59	0.59	0.59	0.59
Yb	3.91	3.63	2.07	6.32	7.06	3.06	3.26	4.06	4.12	4.21	4.19
Lu	0.61	0.54	0.34	0.96	1.06	0.35	0.44	0.54	0.61	0.68	0.69

Major elements in wt.%, trace elements in ppm. LOI = loss on ignition at 1100 °C. rig = rhyolitic ignimbrite; ri = rhyolite. bdl = below detection limit. The location number corresponds to the location number in Fig. 2a and b.

https://doi.org/10.5194/egusphere-2026-1092
Preprint. Discussion started: 18 March 2026

Appendix E: Nd isotope data of rhyolite and rhyolitic ignimbrite from the Margečan area (N Croatia) and Kjumberk Hill (E Slovenia)

Table E1 Nd isotope data of rhyolite and rhyolitic ignimbrite from the Margečan area (N Croatia) and Kjumberk Hill (E Slovenia).

Sample	Lithotype	Sm/Nd	$^{147}Sm/^{144}Nd$	$^{143}Nd/^{144}Nd$	$^{143}Nd/^{144}Nd_{(t)}$	$\varepsilon_{Nd(t)}$[a]	Time (t)[b]
GA-3	RI	0.19560	0.118243	0.512250 ($7*10^{-6}$)	0.512061	-5.13	242 Ma
GV-79	RIG	0.28528	0.142461	0.512342 ($6*10^{-6}$)	0.512067	-5.02	243 Ma
GK-1016	RIG	0.24987	0.151052	0.512321 ($8*10^{-6}$)	0.512080	-4.76	242 Ma
MA-11	RIG	0.22316	0.134911	0.512313 ($6*10^{-6}$)	0.512098	-4.42	243 Ma

Errors in brackets for Nd isotopic ratios are given at the 2σ-level. The method of calculating the errors is presented in the analytical techniques chapter. $^{147}Sm/^{144}Nd$ calculated from the ICP-MS concentrations of Sm and Nd following equation: $^{147}Sm/^{144}Nd = (Sm/Nd)*[0.53151+0.14252*^{143}Nd/^{144}Nd]$. [a] Initial $\varepsilon_{Nd(t)}$ calculated assuming $I^{o}_{CHUR} = 0.512638$, $(^{147}Sm/^{144}Nd)^{o}_{CHUR} = 0.1966$, and $\lambda_{Sm} = 6.54*10^{-12}$ a^{-1}. [b]Coresponding time for the initial ε_{Nd} and initial isotopic ratios for Nd. RIG = rhyolitic ignimbrite; RI = rhyolite.

Appendix F: Zircon U-Pb isotopic data for rhyolite and rhyolitic ignimbrite from the Margečan area (N Croatia) and Kjumberk Hill (E Slovenia)

Table F1 Zircon U-Pb isotopic data obtained by LA-ICP-MS for Kjumberk Hill rhyolite sample (GA-1).

		Isotope ratios									Apparent ages (Ma)							
Analysis	U (ppm)	$^{206}Pb/^{204}Pb$	U/Th	$^{206}Pb^*/^{207}Pb^*$	±2s (%)	$^{207}Pb^*/^{235}U$	±2s (%)	$^{206}Pb^*/^{238}U$	±2s (%)	error corr.	$^{206}Pb^*/^{238}U$	±2s (Ma)	$^{207}Pb^*/^{235}U$	±2s (Ma)	$^{206}Pb^*/^{207}Pb^*$	±2s (Ma)	Best age (Ma)	±2s (Ma)
Spot 1	436	102208	1,77	19,61	4,2	0,2658	6,1	0,03783	4,4	0,72	239,4	10,3	239,3	13	239	97,7	**239,4**	**8,3**
Spot 2	320	15322	1,93	17,07	10,3	0,3081	10,7	0,03818	2,9	0,275	241,6	7	272,7	25,7	549,4	225,5	**241,6**	**7**
Spot 3	581	94501	1,65	19,9	4	0,258	5,5	0,03726	3,7	0,678	235,8	8,7	233	11,5	204,7	94	**235,8**	**7,7**
Spot 4	1144	39470	1,34	17,75	6,5	0,3033	7,3	0,03906	3,2	0,441	247	7,8	268,9	17,1	464,3	144,3	**247**	**7,8**
Spot 5	255	23964	3,07	19,54	4,9	0,2683	6,6	0,03805	4,4	0,668	240,7	10,4	241,3	14,2	247,5	113,3	**240,7**	**8,4**
Spot 6	496	26117	1,84	18,07	8	0,2862	9,7	0,03754	5,5	0,568	237,6	12,8	255,5	21,9	424	178	**237,6**	**8,8**
Spot 7	256	148638	2,16	19,81	3,9	0,2665	5,5	0,03832	3,8	0,702	242,4	9,1	239,9	11,7	215,7	90,1	**242,4**	**9,1**
Spot 9	748	38687	1,47	17,1	7,7	0,309	8	0,03835	2,3	0,281	242,6	5,4	273,4	19,3	546,1	168,8	**242,6**	**5,4**
Spot 10	291	35871	2,3	19,48	4,5	0,2834	6,3	0,04006	4,4	0,701	253,2	10,9	253,3	14,1	254,4	102,8	**253,2**	**8,9**
Spot 11	420	65900	1,65	19,76	4,7	0,2618	6	0,03754	3,7	0,62	237,6	8,6	236,1	12,6	221,9	108,6	**237,6**	**8,6**
Spot 12	358	299048	2,26	19,72	4,9	0,2653	5,6	0,03798	2,5	0,458	240,3	6	239	11,8	225,9	114,1	**240,3**	**6**
Spot 13	395	31808	2,18	19,72	4,6	0,2567	5,7	0,03672	3,5	0,606	232,5	7,9	232	11,9	226,6	105,4	**232,5**	**7,9**
Spot 15	283	31805	1,5	20,03	3	0,2674	4,9	0,03887	3,8	0,781	245,8	9,2	240,6	10,4	190,3	70,8	**245,8**	**9,2**
Spot 16	602	170395	1,5	19,54	3,9	0,2734	5,1	0,03877	3,2	0,628	245,2	7,7	245,4	11	247,7	90,6	**245,2**	**7,7**
Spot 17	582	37252	1,15	16,75	9,7	0,3165	10,6	0,03847	4,3	0,403	243,3	10,2	279,2	25,9	591,4	210,5	**243,3**	**8,2**
Spot 18	181	15023	1,88	20,23	5,5	0,2693	6,7	0,03953	3,9	0,582	249,9	9,6	242,1	14,5	167,1	128,2	**249,9**	**9,6**
Spot 19	247	15254	4,3	18,13	6,4	0,2959	7,1	0,03895	3	0,422	246,3	7,2	263,2	16,5	416,5	144	**246,3**	**7,2**
Spot 21	291	170207	2,5	19,61	4,3	0,2761	5,9	0,03929	4	0,683	248,4	9,8	247,6	12,9	239,5	99,1	**248,4**	**9,8**
Spot 22	342	32486	1,83	18,55	7,1	0,2733	8,4	0,03679	4,5	0,537	232,9	10,4	245,3	18,4	365,5	160,4	**232,9**	**8,4**
Spot 24	193	15365	2,78	19,86	5,3	0,2661	7,1	0,03835	4,7	0,663	242,6	11,2	239,5	15,1	209,6	122,8	**242,6**	**9,2**
Spot 25	334	19408	2,47	20,15	4,9	0,2648	6,1	0,03871	3,5	0,585	244,8	8,5	238,5	12,9	176,5	114,6	**244,8**	**8,5**

Table F2 Zircon U-Pb isotopic data obtained by LA-ICP-MS for Margečan rhyolitic ignimbrite sample (MA-11).

		Isotope ratios									Apparent ages (Ma)							
Analysis	U (ppm)	$^{206}Pb/^{204}Pb$	U/Th	$^{206}Pb^*/^{207}Pb^*$	±2s (%)	$^{207}Pb^*/^{235}U$	±2s (%)	$^{206}Pb^*/^{238}U$	±2s (%)	error corr.	$^{206}Pb^*/^{238}U$	±2s (Ma)	$^{207}Pb^*/^{235}U$	±2s (Ma)	$^{206}Pb^*/^{207}Pb^*$	±2s (Ma)	Best age (Ma)	±2s (Ma)
Spot 60R	296	367595	2,80	19,46	0,97	0,2742	1,49	0,03885	1,13	0,76	245,70	2,72	246,10	3,26	249,90	22,41	**245,70**	**2,72**
Spot 61R	477	153471	1,92	19,64	0,77	0,2714	1,19	0,03886	0,91	0,76	245,78	2,20	243,89	2,59	225,73	17,83	**245,78**	**2,20**
Spot 62R	402	139059	2,73	19,32	0,58	0,2682	1,04	0,03779	0,86	0,83	239,11	2,03	241,27	2,24	262,34	13,38	**239,11**	**2,03**
Spot 63R	444	155513	2,55	19,50	0,77	0,2673	1,10	0,03807	0,78	0,71	240,84	1,85	240,54	2,36	237,68	17,86	**240,84**	**1,85**

https://doi.org/10.5194/egusphere-2026-1092
Preprint. Discussion started: 18 March 2026

Spot 65R	453	394216	2,94	19,53	0,65	0,2778	1,11	0,03958	0,90	0,81	250,23	2,21	248,93	2,46	236,65	15,06	**250,23**	**2,21**
Spot 66R	1569	350609	0,91	19,14	0,56	0,2777	1,00	0,03881	0,83	0,83	245,39	2,00	248,91	2,21	282,23	12,91	**245,39**	**2,00**
Spot 67R	216	106116	2,19	19,69	0,99	0,2722	1,58	0,03920	1,23	0,78	247,85	3,00	244,49	3,44	212,33	22,94	**247,85**	**3,00**
Spot 68R	425	164954	1,78	19,50	0,79	0,2732	1,40	0,03891	1,16	0,83	246,10	2,80	245,28	3,05	237,52	18,11	**246,10**	**2,80**
Spot 69R	823	162724	2,45	19,33	0,54	0,2745	1,10	0,03876	0,96	0,87	245,15	2,30	246,35	2,40	257,76	12,33	**245,15**	**2,30**
Spot 71R	1174	2942675	2,04	19,21	0,82	0,2721	1,26	0,03809	0,96	0,76	240,96	2,26	244,32	2,73	276,77	18,70	**240,96**	**2,26**
Spot 72R	252	164491	3,20	19,43	0,96	0,2666	1,42	0,03781	1,06	0,74	239,27	2,48	239,99	3,04	247,07	22,02	**239,27**	**2,48**
Spot 73R	398	88122	1,62	19,40	0,86	0,2647	1,21	0,03753	0,84	0,70	237,50	1,95	238,48	2,56	248,21	19,94	**237,50**	**1,95**
Spot 74R	783	342719	1,87	19,22	0,72	0,2804	1,41	0,03932	1,21	0,86	248,64	2,95	251,05	3,13	273,63	16,54	**248,64**	**2,95**
Spot 75R	403	104868	2,00	19,38	0,75	0,2748	1,15	0,03892	0,86	0,75	246,16	2,09	246,60	2,51	250,73	17,35	**246,16**	**2,09**
Spot 76R	878	207517	1,37	19,40	0,80	0,2777	1,12	0,03933	0,79	0,70	248,65	1,92	248,85	2,48	250,67	18,42	**248,65**	**1,92**
Spot 77R	407	139783	1,96	19,26	1,42	0,2814	1,69	0,03959	0,92	0,55	250,31	2,26	251,79	3,77	265,58	32,52	**250,31**	**2,26**
Spot 79R	702	84983	1,99	19,14	0,94	0,2758	1,43	0,03861	1,08	0,76	244,21	2,60	247,33	3,15	277,06	21,47	**244,21**	**2,60**
Spot 80R	542	133117	2,26	19,70	0,95	0,2684	1,23	0,03864	0,78	0,64	244,43	1,88	241,44	2,64	212,47	22,01	**244,43**	**1,88**
Spot 81R	438	420187	3,96	19,59	0,79	0,2658	1,21	0,03800	0,92	0,76	240,40	2,17	239,35	2,58	229,05	18,18	**240,40**	**2,17**
Spot 83R	477	189116	3,57	19,54	1,00	0,2668	1,34	0,03811	0,88	0,66	241,09	2,09	240,14	2,86	230,80	23,19	**241,09**	**2,09**
Spot 84R	1033	2488578	2,33	19,43	0,66	0,2721	0,94	0,03863	0,67	0,71	244,35	1,60	244,42	2,04	245,13	15,20	**244,35**	**1,60**
Spot 90C	793	88277	1,41	19,18	0,72	0,2728	1,03	0,03830	0,73	0,71	242,31	1,74	244,97	2,24	270,52	16,56	**242,31**	**1,74**
Spot 91C	962	269211	1,65	19,31	0,57	0,2733	1,05	0,03855	0,89	0,84	243,81	2,12	245,38	2,30	260,40	13,12	**243,81**	**2,12**
Spot 92C	405	262540	1,69	19,63	0,93	0,2621	1,56	0,03760	1,25	0,80	237,94	2,93	236,43	3,30	221,34	21,60	**237,94**	**2,93**
Spot 93C	293	48494	2,50	19,63	0,94	0,2619	1,42	0,03774	1,06	0,74	238,80	2,48	236,20	2,99	210,48	21,94	**238,80**	**2,48**
Spot 94C	690	168949	1,93	19,54	0,86	0,2725	1,50	0,03892	1,23	0,82	246,14	2,98	244,71	3,27	230,91	19,83	**246,14**	**2,98**

Appendix G: Variation diagrams for Zr as a differentiation index vs. selected trace elements and REE for the rhyolitic lavas and rhyolitic ignimbrites from the Margečan area (N Croatia) and Kjumberk Hill (E Slovenia)

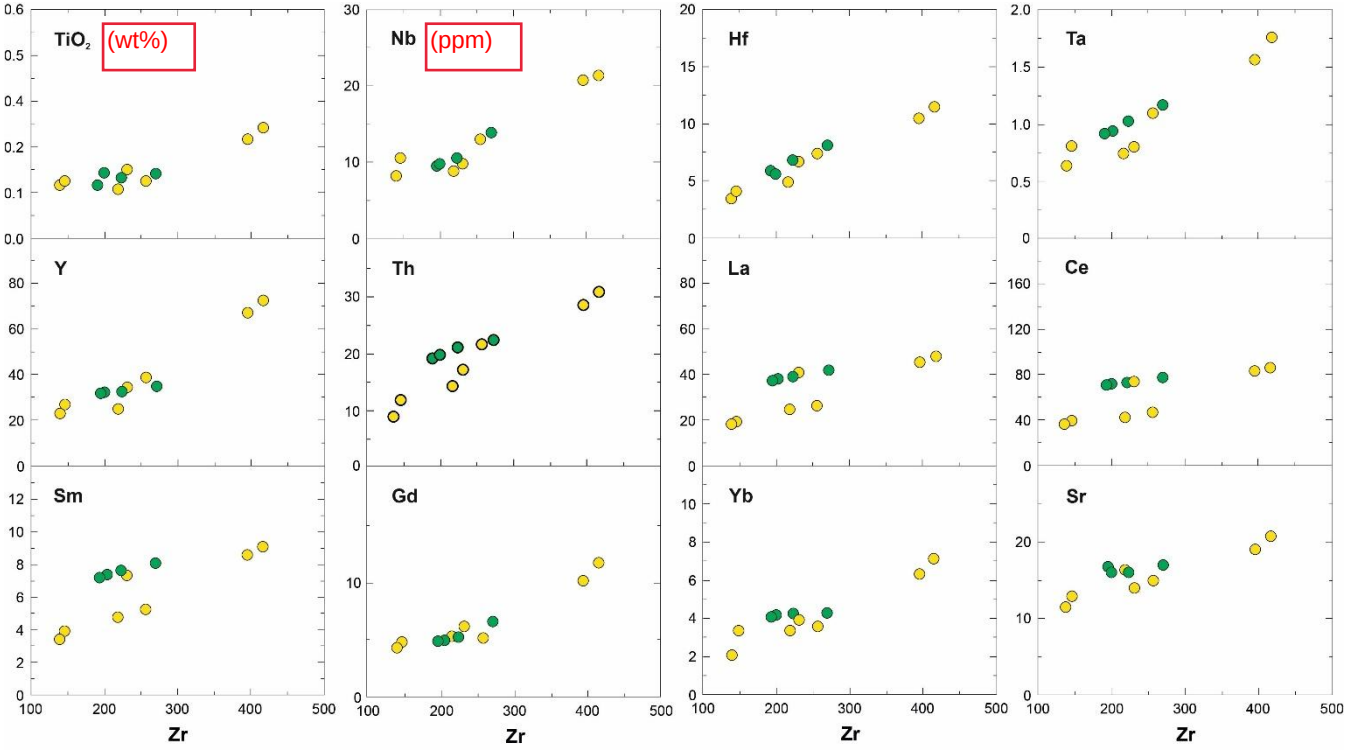

Figure G1 Variation diagrams for Zr as a differentiation index (e.g., Pearce, 1975) vs. selected trace elements and REE for the rhyolitic lavas (green dot) and rhyolitic ignimbrites (yellow dot) from the Margečan area (N Croatia) and Kjumberk Hill (E Slovenia).

Data availability

All data relevant to this study are provided in the Appendices.

https://doi.org/10.5194/egusphere-2026-1092
Preprint. Discussion started: 18 March 2026

Author contributions

Matija Vukovski: writing – original draft, review and editing, conceptualization, formal analysis, investigation, methodology, visualization. Damir Slovenec: writing – original draft, review and editing, data curation, formal analysis, funding acquisition, investigation, project administration, resources, visualization. Mirko Belak: writing – original draft, formal analysis, investigation. Branimir Šegvić: writing – original draft, review and editing, conceptualization, data curation, formal analysis, validation. Ivan Mišur: writing – original draft, data curation, formal analysis. Duje Smirčić: writing – original draft, review and editing, formal analysis, investigation, visualization. Marija Horvat: writing – review and editing, investigation. Duje Kukoč: writing – review and editing, investigation. Tonći Grgasović: writing – review and editing, investigation. Goran Slivšek: writing – original draft, formal analysis.

Competing interests

The authors declare that they have no conflict of interest.

Acknowledgements

Andrew Glore, an undergraduate student at Texas Tech University, is thanked for his assistance with the interpretation of X-ray diffraction data. During the preparation of this work the author(s) used ChatGPT (OpenAI) in order to assist with language editing and formatting of the reference list. After using this tool/service, the author(s) reviewed and edited the content as needed and take(s) full responsibility for the content of the published article.

Financial support

This work was supported by the Croatian Science Foundation under the project “Revealing the Middle Triassic Paleotethyan Geodynamics Recorded in the Volcano-Sedimentary Successions of NW Croatia“ (IP-2019-04-3824) and by the National Recovery and Resilience Plan 2021–2026 of the European Union – NextGenerationEU under the project “Geodynamic evolution of the Dinaridic rift basins in the Middle Triassic“.

References

Altherr, R., Schliestedt, M., Okrusch, M., Seidel, E., Kreuzer, H., Harre, W., Lenz, H., Wendt, I., and Wagner, G. A.: Geochronology of high-pressure rocks on Sifnos (Cyclades, Greece), Contrib. Mineral. Petrol., 70, 245–255, 1979.

Aničić, B., and Juriša, M.: Basic geological map of SFRJ 1:100,000, sheet Rogatec (L 33-68), Institut za geološka istraživanja, Zagreb; Savezni geološki zavod, Beograd, 1984.

https://doi.org/10.5194/egusphere-2026-1092
Preprint. Discussion started: 18 March 2026

Arculus, R. J., and Powell, R.: Source component mixing in the regions of arc magma generation, J. Geophys. Res., 91, 5913–5926, https://doi.org/10.1029/JB091iB06p05913, 1986.

Armstrong, J. T.: Quantitative elemental analysis of individual microparticles with electron beam instruments, in: Electron probe quantitation, edited by Heinrich, K. F. J., and Newbury, D. E., Springer, 261–315, https://doi.org/10.1007/978-1-4899-2617-3_15, 1991.

Atanackov, J., Jamšek Rupnik, P., Jež, J., Celarc, B., Novak, M., Milanič, B., Markelj, A., Bavec, M., and Kastelic, V.: Database of active faults in Slovenia: Compiling a new active fault database at the junction between the Alps, the Dinarides and the Pannonian Basin tectonic domains, Front. Earth Sci., 9, 604388, https://doi.org/10.3389/feart.2021.604388, 2021.

Avanić, R.: Lower Miocene lithostratigraphic units of northwestern Croatia, Ph.D. thesis, University of Zagreb, Croatia, 162 pp., 2012.

Avanić, R., Pavelić, D., Pécskay, Z., Miknić, M., Tibljaš, D., and Wacha, L.: Tidal deposits in the Early Miocene Central Paratethys: The Vučji Jarek and Čemernica members of the Macelj formation (NW Croatia), Geol. Croat., 74, 41–56, https://doi.org/10.4154/gc.2021.06, 2021.

Bachmann, O., and Bergantz, G. W.: Rhyolites and their source mushes across tectonic settings, J. Petrol., 49, 2277–2285, https://doi.org/10.1093/petrology/egn068, 2008.

Bagagli, M., Molinari, I., Diehl, T., Kissling, E., Giardini, D., Clinton, J., Hetényi, G., Graciano, C., Solarino, S., Šipka, V., and AlpArray Working Group: The AlpArray research seismicity-catalogue, Geophys. J. Int., 231, 921–943, https://doi.org/10.1093/gji/ggac226, 2022.

Balázs, A., Matenco, L., Magyar, I., Horváth, F., and Cloetingh, S.: The link between tectonics and sedimentation in back-arc basins: New genetic constraints from the analysis of the Pannonian Basin, Tectonics, 35, 1526–1559, https://doi.org/10.1002/2015TC004109, 2016.

Basch, O.: Basic geological map of Yugoslavia scale 1:100,000, sheet Ivanić-Grad (L 33-81), Geološki zavod, Zagreb; Savezni geološki zavod, Beograd, 1981.

Belak, M., and Tibljaš, D.: Discovery of blueschists in the Medvednica Mountain (Northern Croatia) and their significance for the interpretation of geotectonic evolution of the area, Geol. Croat., 51, 27–32, https://doi.org/10.4154/gc.1998.03, 1998.

Belak, M., Slovenec, D., Schwarz, W. H., Šegvić, B., and Mišur, I.: 40Ar/39Ar ages of glaucophane and phengitic muscovite from orthoblueschists of Mt. Medvednica, NW Croatia: Evidence for Middle–Upper Jurassic subduction in the northwestern segment of the Neotethys, Geol. Carpathica, in review, 2026.

Branney, M. J., and Kokelaar, P.: Pyroclastic density currents and the sedimentation of ignimbrites, Geol. Soc. Lond., Mem., 27, 1–152, https://doi.org/10.1144/GSL.MEM.2003.027, 2002.

Burgissier, A., and Bergantz, G. W.: Reconciling pyroclastic flow and surge: The multiphase physics of pyroclastic density currents, Earth Planet. Sci. Lett., 202, 405–418, https://doi.org/10.1016/S0012-821X(02)00789-6, 2002.

Buser, S.: Basic geological map of SFRY 1:100,000, sheet Celje (L 33-69), Geološki zavod Ljubljana; Savezni geološki zavod, Beograd, 1977.

https://doi.org/10.5194/egusphere-2026-1092
Preprint. Discussion started: 18 March 2026

Buser, S., and Cajhen, J.: Basic geological map of SFRY 1:100,000, sheet Klagenfurt (L 33-53), Geološki zavod Ljubljana; Savezni geološki zavod, Beograd, 1977.

Cas, R. A. F., and Wright, J. V.: Volcanic successions: Modern and ancient, Allen & Unwin, 1987.

Dana, J. D., Klein, C., and Hurlbut, C. S.: Manual of mineralogy, Wiley, 1993.

Deer, W. A., Howie, R. A., and Zussman, J.: An introduction to the rock-forming minerals, 2nd edn., Prentice Hall, 1992.

Ernst, W. G.: A note on phengitic micas from glaucophane schists, Am. Mineral., 48, 1357–1373, 1963.

Faryad, S. W., and Hoinkes, G.: P–T gradient of Eo-Alpine metamorphism within the Austroalpine basement units east of the Tauern Window (Austria), Mineral. Petrol., 77, 129–159, https://doi.org/10.1007/s00710-002-0187-y, 2003.

Ferreiro Mählmann, R., Bozkaya, Ö., Potel, S., Le Bayon, R., Šegvić, B., and Nieto, F.: The pioneer work of Bernard Kübler and Martin Frey in very low-grade metamorphic terranes: Paleo-geothermal potential of variation in Kübler-Index/organic matter reflectance correlations: A review, Swiss J. Geosci., 105, 121–152, https://doi.org/10.1007/s00015-012-0115-3, 2012.

Fodor, L., Jelen, B., Marton, E., Skaberne, D., Čar, J., and Vrabec, M.: Miocene–Pliocene tectonic evolution of the Slovenian Periadriatic fault: Implications for Alpine–Carpathian extrusion models, Tectonics, 17, 690–709, 1998.

Fodor, L., Gerdes, A., Dunkl, I., Koroknai, B., Pécskay, Z., Trajanova, M., Horváth, P., and Vrabec, M.: Miocene emplacement and rapid cooling of the Pohorje pluton at the Alpine–Pannonian–Dinaridic junction, Slovenia, Swiss J. Geosci., 101, 255–271, https://doi.org/10.1007/s00015-008-1286-9, 2008.

Fodor, L., Balázs, A., Csillag, G., Dunkl, I., Héja, G., Jelen, B., Kelemen, P., Kövér, S., Németh, A., Nyíri, D., Selmeczi, I., Trajanova, M., Vrabec, M. A., and Vrabec, M. I.: Crustal exhumation and depocenter migration from the Alpine orogenic margin towards the Pannonian extensional back-arc basin controlled by inheritance, Glob. Planet. Change, 203, 103475, https://doi.org/10.1016/j.gloplacha.2021.103475, 2021.

Frey, M., Hunziker, J. C., Jäger, E., and Stern, W. B.: Regional distribution of white K-mica polymorphs and their phengite content in the Central Alps, Contrib. Mineral. Petrol., 83, 185–197, 1983.

Frisch, W., Dunkl, I., and Kuhlemann, J.: Post-collisional orogen-parallel large-scale extension in the Eastern Alps, Tectonophysics, 327, 239–265, https://doi.org/10.1016/S0040-1951(00)00204-3, 2000.

Garrison, J. M., Davidson, J. P., Minard Hall, M., and Mothes, P.: Geochemistry and petrology of the most recent deposits from Cotopaxi Volcano, Northern Volcanic Zone, Ecuador, J. Petrol., 52, 1641–1678, https://doi.org/10.1093/petrology/egr023, 2011.

Gehrels, G. E., and Pecha, M.: Detrital zircon U–Pb geochronology and Hf isotope geochemistry of Paleozoic and Triassic passive margin strata of western North America, Geosphere, 10, 49, https://doi.org/10.1130/GES00889.1, 2014.

Gehrels, G. E., Valencia, V., and Pullen, A.: Detrital zircon geochronology by laser-ablation multicollector ICP-MS at the Arizona LaserChron Center, Paleontol. Soc. Pap., 12, 67–76, https://doi.org/10.1017/S1089332600001352, 2006.

Gehrels, G. E., Valencia, V., and Ruiz, J.: Enhanced precision, accuracy, efficiency, and spatial resolution of U–Pb ages by laser-ablation–multicollector–inductively coupled plasma–mass spectrometry, Geochem. Geophys. Geosyst., 9, Q03017, https://doi.org/10.1029/2007GC001805, 2008.

https://doi.org/10.5194/egusphere-2026-1092
Preprint. Discussion started: 18 March 2026

Germovšek, C.: Kremenov keratofir pri Veliki Pirešici, Geol., 1, 5–168, 1953.

Germovšek, C.: Triadne predomine severovzhodne Slovenije, Slov. Akad. Znan. Umetn., 1, 1–53, 1959.

Goričan, Š., Halamić, J., Grgasović, T., and Kolar-Jurkovšek, T.: Stratigraphic evolution of Triassic arc–backarc system in northwestern Croatia, Bull. Soc. Géol. Fr., 176, 3–22, https://doi.org/10.2113/176.1.3, 2005.

Gorjanović-Kramberger, D.: Geological and overview map of the Kingdom of Croatia-Slavonia, Zlatak–Krapina, 1:75,000, Zagreb, 1904.

Gorton, M. P., and Shandl, E. S.: From continents to island arcs: A geochemical index of tectonic setting for arc-related and within-plate felsic to intermediate volcanic rocks, Can. Mineral., 38, 1065–1073, https://doi.org/10.2113/gscanmin.38.5.1065, 2000.

Grad, K., and Ferjančič, L.: Basic geological map of SFRY 1:100,000, sheet Kranj (L 33-65), Geološki zavod Ljubljana; Savezni geološki zavod, Beograd, 1974.

Grobe, A., Littke, R., Sachse, V., Urai, J. L., Selverstone, J., von Eynatten, H., and Pleuger, J.: Burial history and thermal maturity of Mesozoic rocks of the Dolomites, Northern Italy, Swiss J. Geosci., 108, 253–271, https://doi.org/10.1007/s00015-015-0187-3, 2015.

Grünthal, G., and Wahlström, R.: The European–Mediterranean Earthquake Catalogue (EMEC) for the last millennium, J. Seismol., 16, 535–570, https://doi.org/10.1007/s10950-012-9302-y, 2012.

Guidotti, C. V., and Sassi, F. P.: Classification and correlation of metamorphic facies series by means of muscovite b data from low-grade metapelites, Neues Jahrb. Mineral. Abh., 153, 363–380, 1986.

Guidotti, C. V., Sassi, F. P., and Blencoe, J. G.: Compositional controls on the a and b cell dimensions of 2M1 muscovite, Eur. J. Mineral., 1, 71–84, 1989.

Halder, M., Paul, M., and Sensarma, S.: Rhyolites in continental mafic Large Igneous Provinces: Petrology, geochemistry and petrogenesis, Geosci. Front., 12, 53–80, https://doi.org/10.1016/j.gsf.2019.07.004, 2021.

Handy, M. R., Schmid, S. M., Bousquet, R., Kissling, E., and Bernoulli, D.: Reconciling plate-tectonic reconstructions of Alpine Tethys with the geological–geophysical record of spreading and subduction in the Alps, Earth Sci. Rev., 102, 121–158, https://doi.org/10.1016/j.earscirev.2010.06.002, 2010.

Handy, M. R., Ustaszewski, K., and Kissling, E.: Reconstructing the Alps–Carpathians–Dinarides as a key to understanding switches in subduction polarity, slab gaps and surface motion, Int. J. Earth Sci., 104, 1–26, https://doi.org/10.1007/s00531-014-1060-3, 2015.

Hawkesworth, C. J., Gallagher, K., Hergt, J. M., and McDermott, F.: Trace element fractionation processes in the generation of island arc basalts, in: Melting and melt movement in the Earth, edited by Cox, K. G., McKenzie, D. P., and White, R. S., Philos. Trans. R. Soc. Lond. A, 342, 179–191, https://doi.org/10.1098/rsta.1993.0008, 1993.

Hofmann, A. W.: Mantle geochemistry: The message from oceanic volcanism, Nature, 385, 219–229, https://doi.org/10.1038/385219a0, 1997.

https://doi.org/10.5194/egusphere-2026-1092
Preprint. Discussion started: 18 March 2026

Hoinkes, G.: Mineralreaktionen und Metamorphosebedingungen in Metapeliten des westlichen Schneebergerzuges und des angrenzenden Altkristallins (Ötztaler Alpen), Tschermaks Mineral. Petrogr. Mitt., 28, 31–54, 1981.

Hughes, C. J.: Spilites, keratophyres, and the igneous spectrum, Geol. Mag., 109, 513–527, https://doi.org/10.1017/S0016756800044741, 1973.

Iwasaki, M., Sassi, F. P., and Zirpoli, G.: New data on the K-white micas from the Sanbagawa Metamorphic Belt, and their petrologic significance, J. Jpn. Assoc. Mineral. Petrol. Econ. Geol., 73, 274–280, 1978.

Janák, M., Froitzheim, N., Yoshida, K., Sasinkova, V., Nosko, M., Kobayashi, T., Hirajima, T., and Vrabec, M.: Diamond in metasedimentary crustal rocks from Pohorje, Eastern Alps: A window to deep continental subduction, J. Metamorph. Geol., 33, 1–20, https://doi.org/10.1111/jmg.12130, 2015.

Kisch, H. J., Sassi, R., and Sassi, F. P.: The b0 lattice parameter and chemistry of phengites from HP/LT metapelites, Eur. J. Mineral., 18, 207–222, https://doi.org/10.1127/0935-1221/2006/0018-0207, 2006.

Kralj, P.: Lithofacies characteristics of the Smrekovec volcaniclastics, northern Slovenia, Geologija, 39, 159–191, https://doi.org/10.5474/geologija.1996.007, 1996.

Kukoč, D., Smirčić, D., Grgasović, T., Horvat, M., Belak, M., Japundžić, D., Kolar-Jurkovšek, T., Šegvić, B., Badurina, L., Vukovski, M., and Slovenec, D.: Biostratigraphy and facies description of Middle Triassic rift-related volcano-sedimentary successions at the junction of the Southern Alps and the Dinarides (NW Croatia), Int. J. Earth Sci., 112, 1175–1201, https://doi.org/10.1007/s00531-022-02259-4, 2023.

Kuljak, G.: Geology of evaporites and accompanying rocks in Kosovo Polje near Knin, Master's thesis, University of Zagreb, Croatia, in Croatian with English abstract, 2004.

Kurz, W., Wölfler, A., Rabitsch, R., and Genser, J.: Polyphase movement on the Lavanttal Fault Zone (Eastern Alps): Reconciling the evidence from different geochronological indicators, Swiss J. Geosci., 104, 323–343, https://doi.org/10.1007/s00015-011-0068-y, 2011.

Linnen, R. L., and Keppler, H.: Melt composition control of Zr/Hf fractionation in magmatic processes, Geochim. Cosmochim. Acta, 66, 3293–3301, https://doi.org/10.1016/S0016-7037(02)00924-6, 2002.

Ludwig, K. R.: User's manual for Isoplot/Ex, version 4.15: A geochronological toolkit for Microsoft Excel, Berkeley Geochronol. Cent. Spec. Publ., 4, 1–245, 2011.

Lustrino, M., Duggen, S., and Rosenberg, C. L.: The Central–Western Mediterranean: Anomalous igneous activity in an anomalous collisional tectonic setting, Earth Sci. Rev., 104, 1–40, https://doi.org/10.1016/j.earscirev.2010.08.002, 2011.

Marci, V., Šćavničar, S., and Sijarić, G.: Petrogenesis of the volcanic rocks of Ivanščica Mt. (River Željeznica), in: X kongres geologa Jugoslavije, Budva, Vol. 1, 329–335, in Croatian with English summary, 1982.

Marci, V., Šćavničar, S., and Sijarić, G.: The new data about volcanic rocks of Ivanščica Mountain, Geološki Vjesnik, 37, 97–104, in Croatian with English abstract, 1984.

Massonne, H. J., and Schreyer, W.: Phengite geobarometry based on the limiting assemblage with K-feldspar, phlogopite, and quartz, Contrib. Mineral. Petrol., 96, 212–224, https://doi.org/10.1007/BF00375235, 1987.

https://doi.org/10.5194/egusphere-2026-1092
Preprint. Discussion started: 18 March 2026

Mioč, P., and Žnidarčič, M.: Basic geological map of SFRY 1:100,000, sheet Slovenj Gradec (L 33-55), Geološki zavod Ljubljana; Savezni geološki zavod, Beograd, 1976.

Mioč, P., Žnidarčič, M., Premru, U., and Nosan, A.: Basic geological map of SFRY 1:100,000, sheet Ravne na Koroškem (L 33-54), Geološki zavod Ljubljana; Savezni geološki zavod, Beograd, 1981.

Niu, Y., and Batiza, R.: Trace element evidence from seamounts for recycled oceanic crust in the eastern Pacific mantle, Earth Planet. Sci. Lett., 148, 471–483, https://doi.org/10.1016/S0012-821X(97)00047-5, 1997.

Niu, Y., Collerson, K. D., Batiza, R., Wendt, J. I., and Regelous, M.: The origin of E-type MORB at ridges far from mantle plumes: The East Pacific Rise at 11°20′, J. Geophys. Res., 104, 7067–7087, https://doi.org/10.1029/98JB02748, 1999.

Okay, A. I.: Jadeite–chloritoid–glaucophane–lawsonite blueschist in north-west Turkey: Unusually high P/T ratios in continental crust, J. Metamorph. Geol., 20, 757–768, 2002.

Okrusch, M., Seidel, E., and Davis, E. N.: The assemblage jadeite–quartz in the glaucophane rocks of Sifnos (Cyclades Archipelago, Greece), Neues Jahrb. Mineral. Abh., 132, 284–308, 1978.

Pamić, J.: Triassic magmatism of the Dinarides in Yugoslavia, Tectonophysics, 109, 273–307, https://doi.org/10.1016/0040-1951(84)90177-6, 1984.

Pamić, J., McKee, E. H., Bullen, T. D., and Lanphere, M. A.: Tertiary volcanic rocks from the Southern Pannonian Basin, Croatia, Int. Geol. Rev., 37, 259–283, https://doi.org/10.1080/00206819509465404, 1995.

Pearce, J. A.: Trace element characteristics of lavas from destructive plate boundaries, in: Andesites, edited by Thorpe, R. S., Wiley, 525–548, 1982.

Pearce, J. A.: A user's guide to basalt discrimination diagrams, in: Trace element geochemistry of volcanic rocks: Applications for massive sulphide exploration, edited by Wyman, D. A., Geol. Assoc. Can. Short Course Notes, 12, 79–113, 1996.

Pearce, J. A., Harris, N., and Tindle, A. G.: Trace element discrimination diagrams for the tectonic interpretation of granitic rocks, J. Petrol., 25, 956–983, https://doi.org/10.1093/petrology/25.4.956, 1984.

Plank, T.: Constraints from thorium/lanthanum on sediment recycling at subduction zones and the evolution of the continents, J. Petrol., 46, 921–944, https://doi.org/10.1093/petrology/egi005, 2005.

Plank, T., and Langmuir, C. H.: The chemical composition of subducting sediment and its consequences for the crust and mantle, Chem. Geol., 145, 325–394, https://doi.org/10.1016/S0009-2541(97)00150-2, 1998.

Premru, U.: Basic geological map of SFRY 1:100,000, sheet Ljubljana (L 33-66), Geološki zavod Ljubljana; Savezni geološki zavod, Beograd, 1982.

Prince, E., Tsukamoto, S., Grützner, C., Vrabec, M., and Ustaszewski, K.: Not too old to rock: ESR and OSL dating reveal Quaternary activity of the Periadriatic Fault in the Alps, Earth Planets Space, 76, 85, https://doi.org/10.1186/s40623-024-02015-6, 2024.

https://doi.org/10.5194/egusphere-2026-1092
Preprint. Discussion started: 18 March 2026

Prince, E., Tsukamoto, S., Grützner, C., Bülhoff, M., and Ustaszewski, K.: Deciphering Pleistocene fault activity in the Eastern Alps: Dating fault gouges with electron spin resonance and optically stimulated luminescence, Tectonics, 44, e2024TC008662, https://doi.org/10.1029/2024TC008662, 2025.

Rainer, T., Sachsenhofer, R. F., Green, P. F., Rantitsch, G., Herlec, U., and Vrabec, M.: Thermal maturity of Carboniferous to Eocene sediments of the Alpine–Dinaric transition zone (Slovenia), Int. J. Coal Geol., 157, 19–38, https://doi.org/10.1016/j.coal.2016.01.003, 2016.

Ratschbacher, L., Frisch, W., Neubauer, F., Schmid, S. M., and Neugebauer, J.: Extension in compressional orogenic belts: The Eastern Alps, Geology, 17, 404–407, 1989.

Ratschbacher, L., Frisch, W., Linzer, H. G., and Merle, O.: Lateral extrusion in the Eastern Alps. Part 2: Structural analysis, Tectonics, 10, 257–271, https://doi.org/10.1029/90TC02623, 1991.

Rieder, M., Cavazzina, G., D'Yakonov, Y. S., Frank-Kamenetskii, V., Gottardi, G., Guggenheim, S., Koval, P. V., Müller, G., Neiva, A. M. R., Radoslovich, E. W., Robert, J., Sassi, F. P., Takeda, H., Weiss, Z., and Wones, D. R.: Nomenclature of the micas, Can. Mineral., 36, 905–912, 1998.

Riley, T. R., Leat, P. T., Pankhurst, R. J., and Harris, C.: Origins of large-volume rhyolitic volcanism in the Antarctic Peninsula and Patagonia by crustal melting, J. Petrol., 42, 1043–1065, https://doi.org/10.1093/petrology/42.6.1043, 2001.

Rollinson, H. R.: Using geochemical data: Evaluation, presentation, interpretation, Longman, 1993.

Rudnick, R. L., and Gao, S.: Composition of the continental crust, in: Treatise on geochemistry, 2nd edn., edited by Holland, H. D., and Turekian, K. K., Elsevier, 1–51, https://doi.org/10.1016/B978-0-08-095975-7.00301-6, 2014.

Saccani, E., Dilek, Y., Marroni, M., and Pandolfi, L.: Continental margin ophiolites of Neotethys: Remnants of ancient Ocean–Continent Transition Zone (OCTZ) lithosphere and their geochemistry, mantle sources and melt evolution patterns, Episodes, 38, 230–249, https://doi.org/10.18814/epiiugs/2015/v38i4/82429, 2015.

Sachsenhofer, R. F., Jelen, B., Hasenhüttl, C., Dunkl, I., and Rainer, T.: Thermal history of Tertiary basins in Slovenia (Alpine–Dinaride–Pannonian junction), Tectonophysics, 334, 77–99, https://doi.org/10.1016/S0040-1951(00)00291-0, 2001.

Sassi, F. P., and Scolari, A.: The b0 value of the potassic white micas as barometric indicator in low-grade metamorphism of pelitic schists, Contrib. Mineral. Petrol., 45, 143–152, 1974.

Schertl, H.-P., Schreyer, W., and Chopin, C.: The pyrope–coesite rocks and their country rocks at Parigi, Dora Maira Massif, Western Alps: Detailed petrography, mineral chemistry and P–T path, Contrib. Mineral. Petrol., 108, 1–21, 1991.

Schmid, S. M., Fügenschuh, B., Kissling, E., and Schuster, R.: Tectonic map and overall architecture of the Alpine orogen, Eclogae Geol. Helv., 97, 93–117, https://doi.org/10.1007/s00015-004-1113-x, 2004.

Schmid, S. M., Bernoulli, D., Fügenschuh, B., Matenco, L., Schefer, S., Schuster, R., Tischler, M., and Ustaszewski, K.: The Alpine–Carpathian–Dinaridic orogenic system: Correlation and evolution of tectonic units, Swiss J. Geosci., 101, 139–183, https://doi.org/10.1007/s00015-008-1247-1, 2008.

https://doi.org/10.5194/egusphere-2026-1092
Preprint. Discussion started: 18 March 2026

Schmid, S. M., Scharf, A., Handy, M. R., and Rosenberg, C. L.: The Tauern Window (Eastern Alps, Austria): A new tectonic map, with cross-sections and a tectonometamorphic synthesis, Swiss J. Geosci., 106, 1–32, https://doi.org/10.1007/s00015-013-0123-y, 2013.

Schmid, S. M., Fügenschuh, B., Kounov, A., Schuster, R., Tischler, M., and Ustaszewski, K.: Tectonic units of the Alpine collision zone between Eastern Alps and western Turkey, Gondwana Res., 78, 308–374, https://doi.org/10.1016/j.gr.2019.07.005, 2020.

Šćavničar, B., Šćavničar, S., and Šušnjara, A.: The volcanic-sedimentary Middle Triassic in the Suvaja brook area (Mt. Svilaja, Outer Dinarides), Prirodosl. Istraž. Acta Geol., 14, 35–82, in Croatian with English summary, 1984.

Šegvić, B., Slovenec, D., Altherr, R., Babajić, E., Mählmann, R. F., and Lugović, B.: Petrogenesis of high-grade metamorphic soles from the Central Dinaric Ophiolite belt and their significance for the Neotethyan evolution in the Dinarides, Ofioliti, 44, 1–30, https://doi.org/10.4454/ofioliti.v44i1.514, 2019.

Šegvić, B., Slovenec, D., Schuster, R., Babajić, E., Badurina, L., and Lugović, B.: Sm–Nd geochronology and petrologic investigation of a sub-ophiolite metamorphic sole from the Dinarides (Krivaja–Konjuh Ophiolite Complex, Bosnia and Herzegovina), Geol. Croat., 73, 119–130, https://doi.org/10.4154/gc.2020.09, 2020.

Šegvić, B., Slovenec, D., and Badurina, L.: Major and rare earth element mineral chemistry of low-grade assemblages inform dynamics of hydrothermal ocean-floor metamorphism in the Dinaridic Neotethys, Geol. Mag., 160, 444–470, https://doi.org/10.1017/S0016756822001030, 2023.

Šikić, K., Basch, O., and Šimunić, A.: Basic geological map of SFRY 1:100,000, Zagreb sheet (L 38-80), Institut za geološka istraživanja, Zagreb; Savezni geološki zavod, Beograd, 1977.

Šimunić, A., Pikija, M., Hećimović, I., and Šimunić, A. I.: Basic geological map of SFRY 1:100,000, explanatory notes for Varaždin sheet (L 33-69), Institut za geološka istraživanja, Zagreb; Savezni geološki zavod, Beograd, 1981.

Šimunić, A., Pikija, M., and Hećimović, I.: Basic geological map of SFRY 1:100,000, Varaždin sheet, Institut za geološka istraživanja, Zagreb; Savezni geološki zavod, Beograd, 1982.

Slovenec, D., and Šegvić, B.: Middle Triassic high-K calc-alkaline effusive and pyroclastic rocks from the Zagorje–Mid-Transdanubian Zone (Mt. Kuna Gora; NW Croatia): Mineralogy, petrology, geochemistry and tectono-magmatic affinity, Geol. Acta, 19, 1–23, https://doi.org/10.1344/GeologicaActa2021.19.2, 2021.

Slovenec, D., Šegvić, B., Halamić, J., Goričan, Š., and Zanoni, G.: An ensialic volcanic arc along the northwestern edge of Palaeotethys—Insights from the Mid-Triassic volcanosedimentary succession of Ivanščica Mt. (northwestern Croatia), Geol. J., 55, 4324–4351, https://doi.org/10.1002/gj.3664, 2020.

Slovenec, D., Horvat, M., Smirčić, D., Belak, M., Badurina, L., Kukoč, D., Grgasović, T., Byerly, K., Vukovski, M., and Šegvić, B.: On the evolution of Middle Triassic passive margins of the Greater Adria Plate: Inferences from the study of calc-alkaline and shoshonitic tuffs from NW Croatia, Ofioliti, 58, 31–46, https://doi.org/10.4454/ofioliti.v48i1.560, 2023.

Slovenec, D., Šegvić, B., and Belak, M.: Petrogenesis of the Middle Triassic bimodal mafic–felsic volcanic suite from the transitional zone of the Southern Alps and the Dinarides (NW Croatia, E Slovenia), in review, 2026.

https://doi.org/10.5194/egusphere-2026-1092
Preprint. Discussion started: 18 March 2026

Smirčić, D., Kolar-Jurkovšek, T., Aljinović, D., Barudžija, U., Jurkovšek, B., and Hrvatović, H.: Stratigraphic definition and correlation of the Middle Triassic volcaniclastic facies in the External Dinarides: Croatia and Bosnia and Herzegovina, J. Earth Sci., 29, 864–878, https://doi.org/10.1007/s12583-018-0789-1, 2018.

Smirčić, D., Vukovski, M., Slovenec, D., Kukoč, D., Šegvić, B., Horvat, M., Belak, M., Grgasović, T., and Badurina, L.: Facies architecture, geochemistry and petrogenesis of Middle Triassic volcaniclastic deposits of Mt. Ivanščica (NW Croatia): Evidence of bimodal volcanism in the Alpine–Dinaridic transitional zone, Swiss J. Geosci., 117, https://doi.org/10.1186/s00015-024-00453-8, 2024.

Sokač, B., Nikler, L., Velić, I., and Mamužić, P.: Basic geological map of SFRY 1:100,000, Gospić sheet (L 33-127), Institut za geološka istraživanja; Savezni geološki zavod, 1974.

Storey, B. C.: The role of mantle plumes in the continental breakup: Case histories from Gondwanaland, Nature, 377, 301–308, https://doi.org/10.1038/377301a0, 1995.

Stucchi, M., Rovida, A., Capera, A. G., Alexandre, P., Camelbeeck, T., Demircioglu, M. B., et al.: The SHARE European earthquake catalogue (SHEEC) 1000–1899, J. Seismol., 17, 523–544, https://doi.org/10.1007/s10950-012-9335-2, 2012.

Sun, S. S., and McDonough, W. F.: Chemical and isotopic systematics of oceanic basalts: Implications for mantle composition and processes, in: Magmatism in ocean basins, Geol. Soc. Lond. Spec. Publ., 42, 313–345, Geol. Soc. Lond., https://doi.org/10.1144/gsl.sp.1989.042.01.19, 1989.

Swinden, H. S., Jenner, G. A., Fryer, B. J., Hertogen, J., and Roddick, J. C.: Petrogenesis and paleotectonic history of the Wild Bight Group, an Ordovician rifted island arc in central Newfoundland, Contrib. Mineral. Petrol., 105, 219–241, https://doi.org/10.1007/BF00678987, 1990.

Tappert, M. C., Rivard, B., Giles, D., Tappert, R., and Mauger, A.: The mineral chemistry, near-infrared, and mid-infrared reflectance spectroscopy of phengite from the Olympic Dam IOCG deposit, South Australia, Ore Geol. Rev., 53, 26–38, https://doi.org/10.1016/j.oregeorev.2012.12.006, 2013.

Tari, G.: Alpine tectonics of the Pannonian basin, doctoral dissertation, Rice University, 1994.

Taylor, S. R., and McLennan, S. M.: The continental crust: Its composition and evolution, Blackwell Sci. Publ., 1985.

Thöni, M.: Dating eclogite-facies metamorphism in the Eastern Alps—Approaches, results, interpretations: A review, Mineral. Petrol., 88, 123–148, https://doi.org/10.1007/s00710-006-0153-5, 2006.

Tomljenović, B., and Csontos, L.: Neogene–Quaternary structures in the border zone between Alps, Dinarides and Pannonian Basin (Hrvatsko zagorje and Karlovac basins, Croatia), Int. J. Earth Sci., 90, 560–578, https://doi.org/10.1007/s005310000176, 2001.

Tomljenović, B., Csontos, L., Márton, E., and Márton, P.: Tectonic evolution of the northwestern Internal Dinarides as constrained by structures and rotation of Medvednica Mountains, North Croatia, in: Geol. Soc. Lond. Spec. Publ., 298, 145–167, Geol. Soc. Lond., https://doi.org/10.1144/SP298.8, 2008.

van Gelder, I. E., Matenco, L., Willingshofer, E., Tomljenović, B., Andriessen, P. A. M., Ducea, M. N., Beniest, A., and Gruić, A.: The tectonic evolution of a critical segment of the Dinarides–Alps connection: Kinematic and geochronological

https://doi.org/10.5194/egusphere-2026-1092
Preprint. Discussion started: 18 March 2026

inferences from the Medvednica Mountains, NE Croatia, Tectonics, 34, 1952–1978, https://doi.org/10.1002/2015TC003937, 2015.

van Hinsbergen, D. J. J., and Schouten, T. L. A.: Deciphering paleogeography from orogenic architecture: Constructing orogens in a future supercontinent as thought experiment, Am. J. Sci., 321, 955–1031, https://doi.org/10.2475/06.2021.09, 2021.

van Hinsbergen, D. J. J., Torsvik, T. H., Schmid, S. M., Maţenco, L. C., Maffione, M., Vissers, R. L. M., Gürer, D., and Spakman, W.: Orogenic architecture of the Mediterranean region and kinematic reconstruction of its tectonic evolution since the Triassic, Gondwana Res., 81, 79–229, https://doi.org/10.1016/j.gr.2019.07.009, 2020.

von Blanckenburg, F., and Davies, J. H.: Slab breakoff: A model for syncollisional magmatism and tectonics in the Alps, Tectonics, 14, 120–131, https://doi.org/10.1029/94TC02051, 1995.

von Blanckenburg, F., Kagami, H., et al.: The origin of Alpine plutons along the Periadriatic Lineament, Schweiz. Mineral. Petrogr. Mitt., 78, 57–68, https://doi.org/10.5169/seals-59274, 1998.

Vrabec, M.: Style of postsedimentary deformation in the Plio-Quaternary Velenje basin, Slovenia, Neues Jahrb. Geol. Paläontol. Monatsh., 1999(8), 449–463, https://doi.org/10.1127/njgpm/1999/1999/449, 1999.

Vrabec, M., and Fodor, L.: Late Cenozoic tectonics of Slovenia: Structural styles at the Northeastern corner of the Adriatic microplate, in: The Adria microplate: GNSS geodesy, tectonics and hazards, NATO Sci. Ser. IV: Earth Environ. Sci., 61, 151–168, Springer, https://doi.org/10.1007/1-4020-4235-3_10, 2006.

Vukovski, M.: Structural-geological setting of Ivanščica Mountain and its tectonic position at the junction of the Alps, Dinarides and Pannonian Basin, Ph.D. thesis, University of Zagreb, Croatia, 146 pp., 2024.

Vukovski, M., Špelić, M., Kukoč, D., Troskot-Čorbić, T., Grgasović, T., Slovenec, Da., and Tomljenović, B.: Unravelling the tectonic evolution of the Dinarides–Alps–Pannonian Basin transition zone: Insights from structural analysis and low-temperature thermochronology from Ivanščica Mt., NW Croatia, Swiss J. Geosci., 117, 16, https://doi.org/10.1186/s00015-024-00464-5, 2024.

Wadsworth, F. B., Llewellin, E. W., Vasseur, J., Gardner, J. E., and Tuffen, H.: Explosive–effusive volcanic transitions caused by sintering, Sci. Adv., 6, eaba7940, https://doi.org/10.1126/sciadv.aba7940, 2020.

Wang, Q., Chung, S. L., Li, X. H., Wyman, D., Li, Z. X., Sun, W. D., Qiu, H. N., Liu, Y. S., and Zhu, Y. T.: Crustal melting and flow beneath northern Tibet: Evidence from Mid-Miocene to Quaternary strongly peraluminous rhyolites in the Southern Kunlun Range, J. Petrol., 53, 2523–2566, https://doi.org/10.1093/petrology/egs058, 2012.

Weber, J., Vrabec, M., Stopar, B., Pavlovčič-Prešeren, P., and Dixon, T.: The Pivo-2003 experiment: A GPS study of Istria Peninsula and Adria microplate motion, and active tectonics in Slovenia, in: The Adria microplate: GPS geodesy, tectonics and hazards, NATO Sci. Ser. IV: Earth Environ. Sci., 61, 305–320, Springer, https://doi.org/10.1007/1-4020-4235-3_21, 2006.

Whitney, D. L., and Evans, B. W.: Abbreviations for names of rock-forming minerals, Am. Mineral., 95, 185–187, https://doi.org/10.2138/am.2010.3371, 2010.

https://doi.org/10.5194/egusphere-2026-1092
Preprint. Discussion started: 18 March 2026

Wilson, M.: Igneous petrogenesis, Unwin Hyman, 1989.

Wölfler, A., Kurz, W., Danišík, M., and Rabitsch, R.: Dating of fault zone activity by apatite fission track and apatite (U-Th)/He thermochronometry: A case study from the Lavanttal fault system (Eastern Alps), Terra Nova, https://doi.org/10.1111/j.1365-3121.2010.00943.x, 2010.

Wölfler, A., Kurz, W., Fritz, H., and Stüwe, K.: Lateral extrusion in the Eastern Alps revisited: refining the model by thermochronological, sedimentary and seismic data, Tectonics, 30, TC4006, https://doi.org/10.1029/2010TC002782, 2011.

Workman, R. K., and Hart, S. R.: Major and trace element composition of the depleted MORB mantle (DMM), Earth Planet. Sci. Lett., 231, 53–72, https://doi.org/10.1016/j.epsl.2004.12.005, 2005.

Xu, Y. G., Chung, S. L., Shao, H., and He, B.: Silicic magmas from the Emeishan large igneous province, Southwest China: Petrogenesis and their link with the end-Guadalupian biological crisis, Lithos, 119, 47–60, https://doi.org/10.1016/j.lithos.2010.04.013, 2010.

Žibret, L., and Vrabec, M.: Palaeostress and kinematic evolution of the orogen-parallel NW–SE striking faults in the NW External Dinarides of Slovenia unraveled by mesoscale fault-slip data analysis, Geol. Croat., 69, 295–305, https://doi.org/10.4154/gc.2016.30, 2016.